Infrared Studies of Gas Phase and Surface Processes of the Enhancement of Catalytic Methane Decomposition by Low Temperature Plasma

A. J. Knoll*, S. Zhang, M. Lai, P. Luan, and G. S. Oehrlein*

Department of Materials Science and Engineering and the Institute for Research in Electronics and Applied Physics, University of Maryland, College Park, MD 20742, USA

*Corresponding authors: knollaj@umd.edu, oehrlein@umd.edu

Abstract

Catalyst enhancement by atmospheric pressure plasma is a recently emerging field of research that embodies a complex system of reactive species and how they interact with surfaces. In this work we use an atmospheric pressure plasma jet integrated with a nickel on Al_2O_3/SiO_2 support catalyst material to decompose methane gas by partial oxidation reaction. We use Fourier-transform Infrared spectroscopy (FTIR) analysis of the gas phase post reaction to measure the loss of methane and the production of CO, CO_2, and H_2O and diffuse reflectance Fourier-transform Infrared spectroscopy (DRIFTs) *in situ* analysis of the catalyst surface as a function of both catalyst temperature and plasma operating parameters. We find reduction of methane by both plasma alone, catalyst alone, and an increase when both plasma and catalyst were simultaneously used. The production of CO appears to be due primarily to the plasma source as it only appears above 2.5 W plasma dissipated power and decreases as catalyst temperature increases. CO_2 production is enhanced by having the catalyst at high temperature and H_2O production depends on both plasma power and temperature. Using DRIFTs we find that

both heating and plasma treatment remove absorbed water on the surface of the catalyst. Plasma treatment alone however leads to the formation of CO and another IR spectral feature at 1590 cm^{-1}, which may be attributed to carboxylate groups, bonded to the catalyst surface. These species exhibit a regime of plasma treatment where they are formed on the surface and where they are significantly removed from the catalyst surface. We see the formation of a new spectral feature at 995 cm^{-1} and discuss the behavior and possible origins of this feature. This research highlights the potential for plasma regeneration of catalyst materials as well as showing enhancement of the catalytic behavior under low temperature plasma treatment.

1. Introduction

The understanding of cold atmospheric plasma (CAP) – surface interaction is essential for the advancement of the emerging field of plasma enhanced catalysis.[1,2,3] The synergistic enhancement of catalysts by CAP has recently drawn great amount of research attention due to its potential for reducing catalyst energy demands, allowing new materials to be used as catalysts, and even the regeneration of catalysts currently used catalyst materials to extend their lifetimes.[3] This emerging technology has so far been applied to several applications toward environmental solutions such as the destruction of chlorofluorocarbons,[2] removal of volatile organic compounds such as toluene and NO_x which are air pollutants.[4,5] As a model plasma-catalysis system that we will further explore in this work, the decomposition or oxidation of methane into hydrogen gas and CO_x species is being investigated for the goal of capturing the hydrogen for efficient syngas production[6] and also for the goal of removal of methane from the environment prior to release into the atmosphere where it acts as a very strong greenhouse gas.[7]

In the field of atmospheric pressure plasma interactions with catalyst materials, plasma-catalyst synergistic effects are of great interest. One specific phenomenon seen from plasma treatment of catalyst is the shift of the curve of decomposition of material vs temperature to a lower temperature range.[2,8,9] Whitehead et al. take this study one step further to show that the amount of temperature difference between the plasma and non-plasma treatment converted to the same amount of electrical energy would take far more energy than the plasma treatment requires.[2] For the 50% decomposition of methane point using only heating of the catalyst it would take 60 watts more energy than for a plasma catalysis combined approach. In order to reduce 60 watts of thermal energy from the

system, the plasma source only uses 1 watt of energy to accomplish this task saving significant energy. They also confirm from separate plasma and thermal catalysis treatments that they only achieve ~20% decomposition whereas when the plasma is brought in contact with the catalyst the decomposition increases to ~65%. Another effect of plasma enhancement of catalysis is the change of the selectivity of the reaction products. Pietruszka et al. demonstrated that increasing the input power of the plasma treatment during catalysis leads to an increase in the CO_2 vs CO selectivity for a methane decomposition reaction.[10] They attribute this to moving closer to the thermodynamic equilibrium for CO_2 production using plasma input energy which normally requires a much higher temperature than used for the plasma treatment.

While some effects of the plasma on catalysis are clear, there is a much more limited amount of research focused on the actual surface reactions that cause synergistic effects.[3] The possible synergistic effects at the surface of the catalysts have been outlined in a review paper by Neyts et al..[11] The surface morphology[12] and dispersion of the catalyst material[13] on the support structure have been shown to change post plasma treatment which could help with the catalyst reaction by leading to more reactive sites. The plasma can also change the chemical state of the catalyst material such as the reduction of NiO to the more reactive Ni which has been shown to possibly occur[14,15] or simply changing the oxidative state of the metal. Additional surface processes can also be modified by plasma exposure such as the reduction of catalyst poisoning by deposition of unwanted surface species. Wang et al. (2013) has shown an increase in NH_3 conversion efficiency using a Fe catalyst from ~7 % for both plasma and catalysis alone to a 99% conversion efficiency by a combined approach, which is possibly due to the plasma

induced prevention of surface bound nitrogen that destroys catalyst reactive sites.[16] There are also potential catalyst effects on the plasma that may occur for some systems which can help synergistic effects, though these effects are less likely to occur for our experimental system.[17] We believe that investigations are required to evaluate specific surface effects during the direct plasma interaction with the catalyst surface. These insights are expected to be crucial for further understanding of what synergistic effects occur for plasma catalysis systems.

There are several approaches to the conversion of methane over catalyst materials. The most commonly used one for hydrogen production currently is reacting methane with steam to produce CO, CO_2 and H_2 which is an endothermic process requiring 206 kJ/mol of energy and is shown in equation 3. Another reaction is the typical combustion reaction in which methane reacts with 2 O_2 species to produce CO_2 and H_2O, however this reaction is highly exothermic and releases ~800 kJ/mol of energy (see equation 2). Methane can react with CO_2 to produce CO and H_2 but this approach requires a large energy input of 247.4 kJ/mol which is larger than steam reformation and is shown in equation 4. The approach that is most desirable for our work which can be done at lower temperatures is the partial oxidation of methane which is mildly exothermic releasing 35.6 kJ/mol and is described in equation 1.[4]

$$CH_4 + 0.5O_2 \Rightarrow CO + 2H_2 \quad (1)$$

$$CH_4 + 2O_2 \Rightarrow CO_2 + 2H_2O \quad (2)$$

$$CH_4 + H_2O \Rightarrow 2CO + 3H_2 \quad (3)$$

$$CH_4 + CO_2 \Rightarrow 2CO + 2H_2 \quad (4)$$

$$CO + H_2O \Rightarrow CO_2 + H_2 \quad (5)$$

It should be noted that any CO produced can undergo several reactions post plasma exposure with oxygen and water vapor to form CO_2. The first of these reactions with oxygen only produces CO_2 and the other reaction produces both CO_2 and H_2 as shown in equation 5. This means that CO is one of the more difficult species to produce generally as it can react to form the other products of the partial oxidation reaction as well. However, the above reactions generally do not take into account a plasma environment which is highly non-equilibrium and may favor reactions not typically seen for methane conversion. Some of these species include atomic oxygen which is reactive enough to break the bonds between many other molecular species, CH_x species where x is less than 4 which normally occurs at a surface but can happen in the gas phase of a plasma environment, and metastable species such as excited CO_2 which can absorb significant vibrational energy.

The goal of this work is to establish the methodology that allows for careful study of catalyst materials as they are exposed to plasma based reactive species and undergoing catalyst reactions. Jia et al.[18] develop a unique plasma source to investigate in situ surface changes using a direct IR beam and compare it to a known plasma source investigated by ex-situ DRIFTs, which provides excellent surface analysis, but has difficulty comparing the two plasma sources directly. In our work we develop a technique to look at the surface changes and catalyst effectiveness in situ with the sample plasma source which removes possibility of changes with changing plasma source. Rodrigues et al.[19] also

develops the innovative surface chemistry measurements by DRIFTs for a plasma system by building a plasma source into the DRIFTs setup dome where the catalyst is held. Our experimental setup seeks to follow a very similar approach to this paper but instead incorporating a well characterized plasma jet into this DRIFTs dome. Stere et al.[17,20] described an infrared-based approach to study the effect of plasma generated by Helium based ring style reactor on Al_2O_3 supported Ag catalytic processes for the decomposition of toluene and n-octane . This work does a good job at surface analysis, but they use a plasma source based on helium which significantly increases operation costs compared with a source that uses argon and therefore argon needs to be further investigated.

In this work, we adopt a similar approach which utilizes a well characterized RF powered Ar fed atmospheric pressure plasma jet source with comprehensive surface characterization techniques to monitor a nickel catalyst plus plasma system for the decomposition of methane. We use nickel catalyst due to its common use in the literature for similar applications and the fact that it is an earth abundant material which has some room for improvement in its use as a catalyst compared to some rarer earth metals. For example, nickel has been used in the literature for dry reformation of methane by Swaan et al.[21], Ruckenstein et al.[22], Guo et al.[23], and Bradford et al.[24] Using DRIFTs, we can monitor changes to the surface that are sensitive to IR absorption and observe these changes as they occur in real time. This setup is then connected to a gas cell which uses IR absorption to monitor several critical species involved in the reaction and the products of the methane partial oxidation reaction. While CO is expected as a product from this reaction, it is also possible to form CO_2 and H_2O depending on the amount of available oxygen, catalyst surface states, and energetic particles produced from the plasma source.

We are able to monitor how these species are produced relative to one another based on plasma and catalyst conditions and also monitor the reduction in methane amount which reveals the effectiveness of the methane conversion by this system. Enhancement of the catalyst reaction by plasma will be investigated through methane reduction by studying the difference between a) plasma alone, b) catalyst alone, and c) combined action of plasma interacting with the catalyst material. The gas phase results are then compared to what changes occur on the catalyst surface which may help suggest possible enhancements mechanisms. For instance, carbon deposition on a catalyst surface which is strongly bonded and is not removed quickly by the catalytic reaction can lead to a loss of reactive sites on the catalyst material called catalyst poisoning. This can be monitored by the DRIFTs to see under what conditions this may occur for the catalyst material and if it is possible for the plasma to remove any of these species to regenerate the catalyst. It is critical to understand the behavior of these catalyst surface changes in detail since this may suggest further catalyst materials for future plasma enhancement work.

2. Experimental Procedures

2.1 Plasma source

The plasma source used in this work is a MHz driven design created by Bruggeman *et al*. and has been extensively characterized for plasma species produced, heating, and gas flow parameters.[25,26,27] The design uses a 1 mm diameter tungsten pin electrode mounted inside a quartz tube (1.5 mm inner diameter (ID) and 3 mm outer diameter (OD)) with a grounded copper ring electrode (5.3 mm length, 3 mm ID). The original design is based on the atmospheric pressure plasma jet (APPJ) proposed by Park and Selwyn.[28] The standard operating conditions of the MHz jet are a 14.4 MHz modulated driven frequency with a 20% on/off duty cycle (20% on time, 80% off time). Details of how the power was calculated for this source can be found in previous work.[29] The gas flow in this work has been reduced from the original standard flow of 1.5 liter per minute (lpm) to 0.4 lpm Ar flow through the jet in order to increase the residence time of the reactant gases in the proximity of the catalyst material. The gas flow of the plasma source cannot be lowered below this point because this will lead to greatly increased heating of the plasma source and ignition of the jet becomes difficult below approximately 0.4 lpm. Additionally, lowering the gas flow to lower values will lead to a larger discrepancy between previous work where this plasma source has been characterized. The methane used for this work has a purity of 99.99%.

2.2 Catalyst Preparation

The catalyst material used in this work is a nickel-based catalyst supported on a combination of Al_2O_3 and SiO_2 and is in the form of a fine powder. The weight percentage of nickel is 65% and has a surface area of ~175 m^2/g. This catalyst was purchased from Sigma Aldrich. The catalyst is in the form of a powder with a particle

size ranging from 100-500 μm. The catalyst specifically used was sifted through metal meshes of 150 μm and 250 μm to narrow the size distribution of the powder used. The exact morphology of the powder is unknown and effect of plasma treatments on morphology was not studied directly in this work. Due to the experimental setup involving a slanted gas flow from the plasma jet and the powder being very fine, the powder was pressed into ball shaped pellets around a ceramic center approximately 6 mm in diameter which is the diameter of the inner reaction chamber of the DRIFTs reaction chamber. Tests were done to show that the catalyst material is stable under the gas flow conditions of the plasma jet and that no catalyst materials were removed from the pellet. This material configuration was used for both gas phase and DRIFTs results for consistency.

2.3 Characterization and Experimental Setup

The characterization setup is based on an FTIR system (IRTracer-100, Shimadzu) with a liquid nitrogen cooled mercury cadmium telluride (MCT) detector. For the gas phase measurements, a custom-built gas cell was used as shown in Figure 1 which is made from quartz and ZnSe windows. All gas phase measurements are done at 0.5 cm^{-1} resolution, Box-Car apodization and with 3 scans averaged together to allow for good time resolution investigating real time changes.

The surface of catalysts was characterized using the same FTIR system along with a DRIFTs accessory (Praying Mantis , Harrick Scientific) and a high temperature reaction chamber (HVC-DRM-5) which was used for temperature and environment control around the catalyst sample. The reaction chamber has two KBr windows for IR

light a 3rd viewport which was converted into a ceramic feedthrough for the integration of RF plasma jet as pictured in Figure 1. All measurements done with the DRIFTs cell use 4 cm^{-1} resolution, Happ-Genzel apodization, and 20 scans averaged for each measurement. The optimized DRIFTs signal was approximately 10 E based on the monitor setting of the Shimadzu FTIR software.

The experimental setup for the plasma catalyst interaction was kept consistent between the gas phase and the DRIFTs experiments to ensure uniformity. The distance of the viewport window where the plasma jet source, or APPJ for short, is located to the middle of the DRIFTs heated reactor is approximately 8 mm and at an angle of 40°. The distance of the plasma jet can be changed by altering the ceramic feed through piece so that the distance from the tip of the nozzle to the catalyst is the only parameter changing when varying distance. The distance from the end of the plasma nozzle to the grounded electrode and the high voltage pin are kept the same for all experimental conditions as shown in Figure 1. The gas through the plasma jet is 0.4 lpm Ar with a 0.5% admixture of O_2 gas and there is another gas flow from the bottom of the high temperature reaction chamber which is 200 sccm Ar with 4 sccm CH_4. The gas is then mixed in the reaction chamber above the catalyst prior to entering the heated catalyst area. The entire high temperature reactor is water cooled to keep the metal, windows, and plasma jet cooled to prevent thermal damage during experiments. The plasma jet was operated to avoiding an arcing state in order to keep the plasma conditions as similar as possible to the plasma state without a surface involved.

The experimental procedure for all experiments involved a conditioning step of the plasma source prior to use with the catalyst to remove any contaminants which may

have been deposited in the source. The gas lines used in the experiments are also pumped using vacuum systems at 1 x 10^{-5} torr pressure for removal of any atmospheric air prior to opening of the gas bottles to ensure purity. The catalyst pellet is then added to the reaction chamber and then the reaction chamber is flushed with the Ar and O_2 gas flows for 20 minutes prior to start of experiments to remove any residual air from the reaction chamber. For experiments not using any catalyst, a ceramic material of approximately the same size as the catalyst material was placed in the reaction chamber as a non-reactive substrate to keep the flow dynamics of the reaction chamber the same. The total volume of the reaction chamber is approximately 8.0 cm^3 and the total volume of the full reaction chamber including the gas area where the catalyst is present is 0.45 cm^3. The actual cup that holds the catalyst sample has an approximate maximum volume of 0.10 cm^3. Since all the gas must flow through the catalyst reaction area the gas residence time in this area is approximately 50 ms. However, the actual gas residence time is likely significantly smaller than this as the catalyst takes up some of this volume through which the gas flows and therefore the velocity will increase. There is some distance of gas line between the DRIFTs cell and the gas phase cell for measurement in the FTIR system to ensure that the gas has cooled to close to room temperature prior to entering the gas cell to reduce any heating effects on the measured spectrum. The chamber is designed so that the plasma extending from the APPJ source is targeted directly at the center of the circular catalyst bed. The reactive species like atomic oxygen, energetic metastable species etc. from the plasma effluent are guided to the catalyst surface. Meanwhile, gas methane flows through catalyst itself, which leads to the interaction of plasma effluent, methane and catalyst itself. The coupling of plasma onto catalyst surface is adjusted by the distance of the

nozzle to catalyst and the power dissipation of the plasma source. Electrical arcing to the metal inside the enclosure was avoided by keeping the power below a level shown to cause arcing as each distance. The visible plume of the plasma is difficult to estimate with this setup and is also not a clear cutoff of ionized species so only nozzle distances were reported.

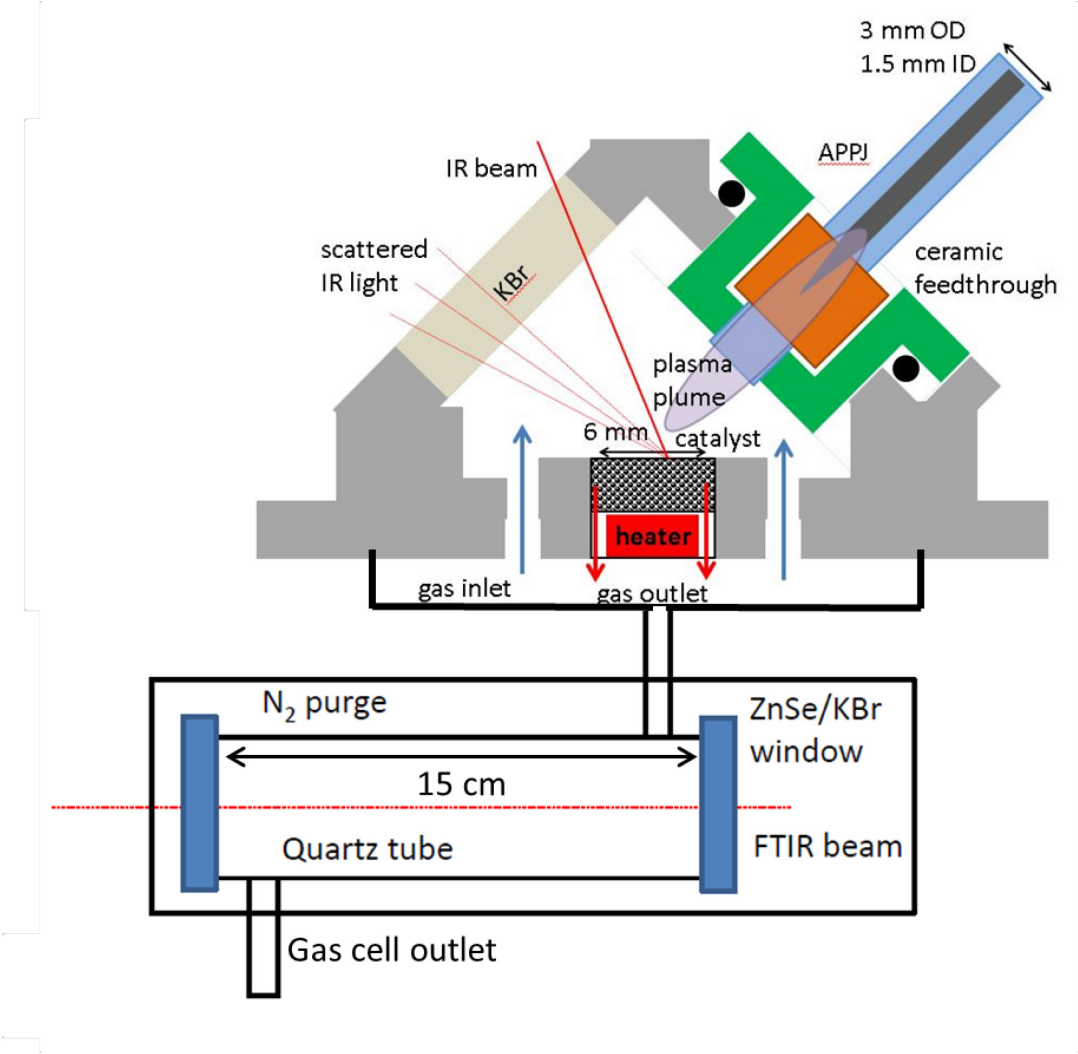

Figure 1: Overview of experimental setups of DRIFTs surface measurements where the plasma treatment of the catalyst occurs and gas phase measurements which are conducted post downstream from the DRIFTs setup.

3. Experimental Results

3.1 Gas Phase Results

The first set of experimental results that were collected focus on the gas phase information. The goal of gas phase measurements is to determine the effectiveness of the methane reduction by plasma catalysis and investigate what species are produced by this catalytic reaction. Specifically, we look at the amount of methane which is reduced by exposing it to the catalyst material, the plasma, or both combined together to see if a synergistic effect occurs by plasma catalyst treatment. The products of this reaction are then examined as well to determine the selectivity of certain species over others, specifically at CO, CO_2, and H_2O which we are able to carefully examine using FTIR.

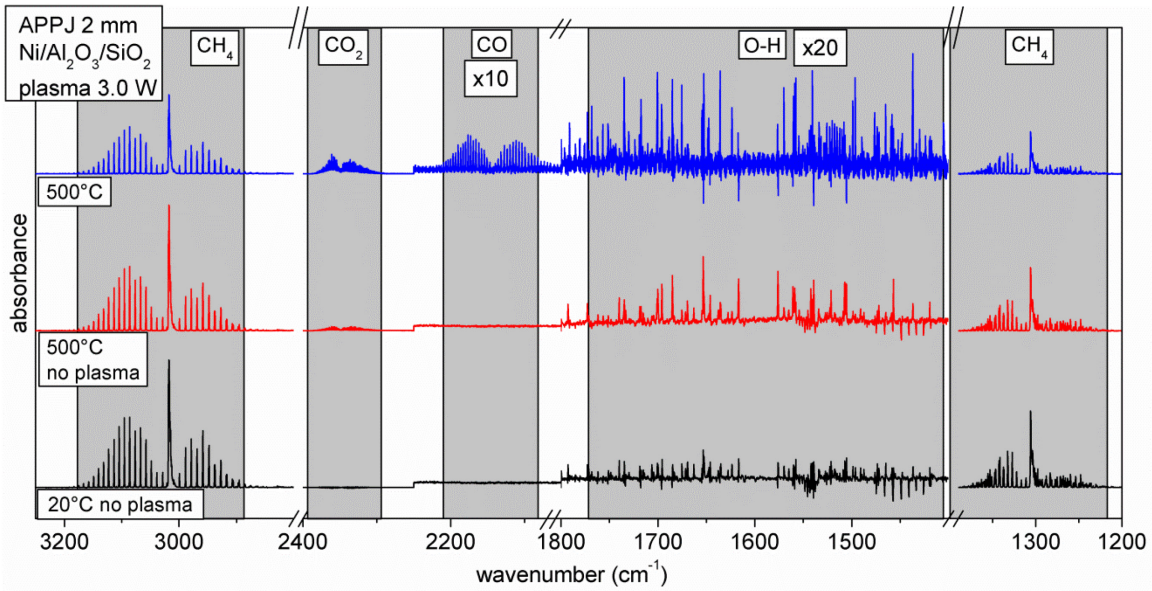

Figure 2: Full spectrum gas phase FTIR for 20 °C no plasma, 500 °C no plasma, and 2 mm plasma 3 W case at 500 °C taken with 0.5 cm^{-1} wavenumber resolution showing the primary complete spectrum which highlights the two CH_4 spectral features, the CO_2 spectrum, the CO spectrum (x10), and the O-H spectrum (x20).

Figure 2 shows the FTIR gas phase results from the 15 cm length gas measurement cell connected to the output from the DRIFTs high temperature reactor setup with the integrated plasma source for the 8 mm plasma treatment distance case. The data shown is for 3 W at 500 °C catalyst temperature compared with no plasma at room temperature. This overview shows the specific regions we will use to calculate the density of each of the gas product species from the catalysis reaction. In order to quantify these peaks, Beer's law of absorbance was applied to the spectrum to convert FTIR absorbance into species density for each of these four species observed in Figure 2. The conversion from absorbance to density is given by equation 1.

$$n = \frac{Abs}{0.4343 * \sigma * l} \quad (1)$$

In this equation n is the density of the species being calculated, Abs is the absorbance measured by FTIR, l is the path length of the gas cell which for this system is 15 cm, and σ is the cross section of each individual peak which were calculated from the HITRAN FTIR data base[30] with additional the correction factors taken from the published works which will be described in detail in the following sub-sections.

3.1.1 CH_4

The first species which is critical for the discussion of the catalyst reaction is methane. The dominant peaks shown here are from the methane gas which is added at ~1% concentration to the Ar/O_2 gas flow through the cell and give rise in the spectrum to two spectral features: one from 3160 to 2900 cm^{-1} which has a number of smaller peaks to either side of a large central peak and corresponds to the stretching of the C-H bonds in the methane and one from 1370 to 1240 cm^{-1} which has a similar structure though it is smaller in absorbance and corresponds to the bending of the C-H bonds in the methane.[31] A highlight of the higher wavenumber spectrum is shown in Figure 3 which is used for the calculation of the CH_4 density. It is immediately clear that while the methane spectrum absorbance is reduced, we are not converting all of the methane present by this method and therefore careful quantitative analysis is needed to measure the change in the amount of methane. We can see the production of several new peaks which correspond to species which are produced by the partial oxidation reaction of methane, as shown in figure 2.

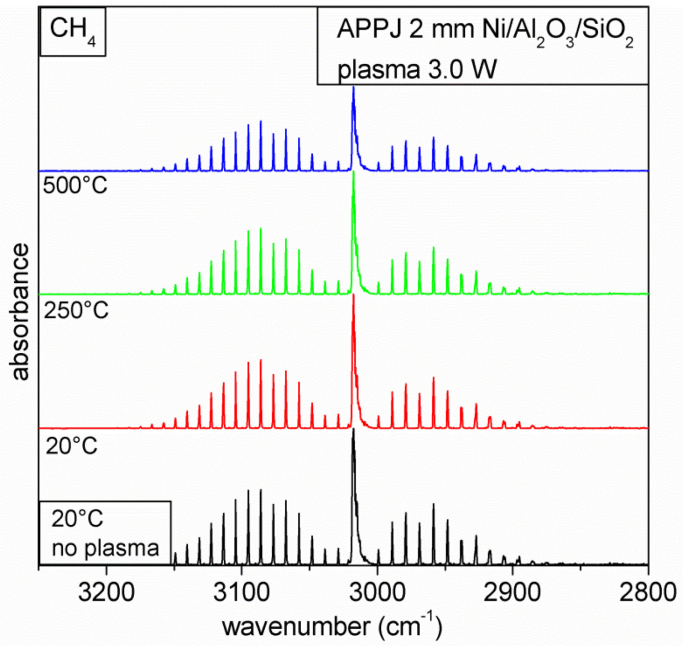

Figure 3: Methane spectrum for 3 W case, 20, 250, and 500 °C showing the individual peaks and demonstrating how methane density is calculated.

For the calculation of the methane density 10 different individual peaks shown in Figure 3 were used to calculate density individually using cross sections for those specific peaks and then these densities were then averaged. The specific peaks used are at 2958.4, 2968.8, 2978.9, 2898.0, 3028.8, 3038.5, 3048.3, 3057.7, 3067.4, 3085.9 cm^{-1}. For the calculated methane density was further calibrated by using mass flow controllers to precisely flow set amounts of methane into the FTIR gas cell and measuring the absorbance for each known concentration of methane. This absorbance was then converted to density and the relationship between the real density and the measured density was found to be linear and then corrected for. This correction factor was then

applied to all data collected with the methane spectrum to give a more accurate estimation of the amount of methane present.

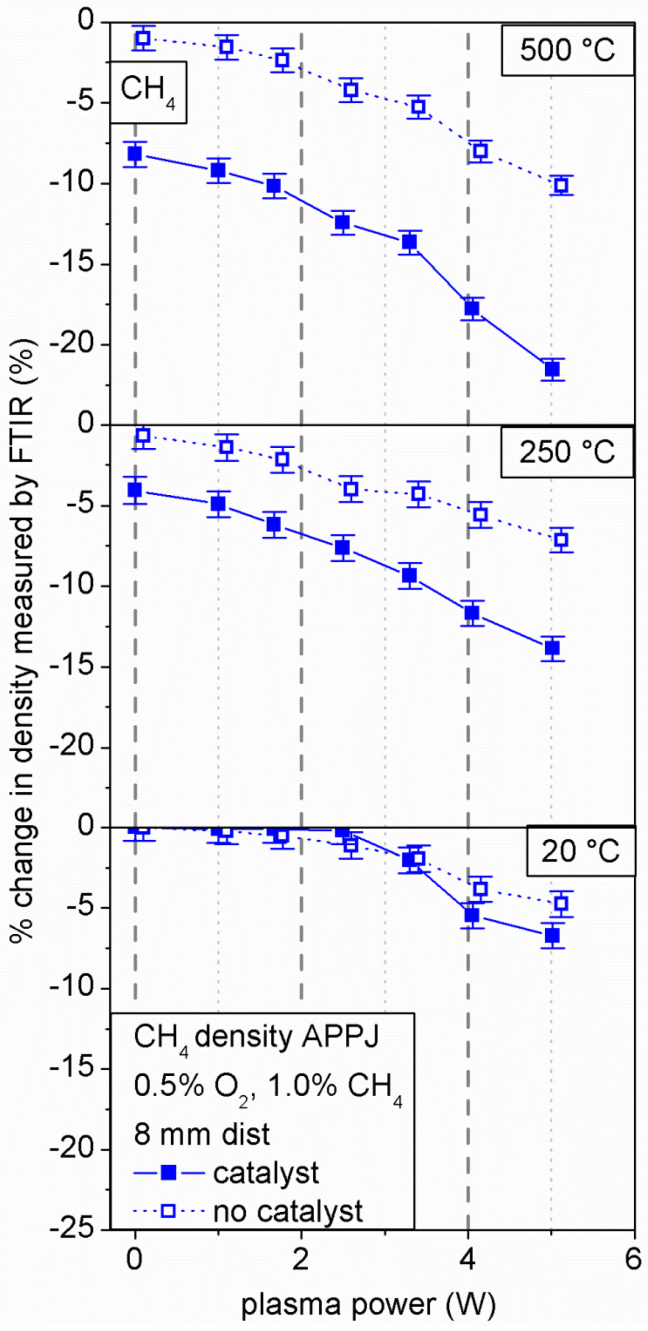

Figure 4: Percentage reduction of CH_4 compared to initial methane density for 500, 250, 20 °C temperatures at 8 mm distance with catalyst and plasma only conditions.

The amount of methane reduction from the starting methane level (in percent) is shown in figure 4 for 8 mm distance. We compare a situation with catalyst vs. no catalyst for a range of plasma powers at three temperatures i.e. 20, 250, 500°C. In general, we see more methane reduction with increasing plasma power. This reduction amount is lower when there is no catalyst present, so the only conversion is occurring by plasma interacting with the gas. Additionally, the amount of methane converted increases with temperature, particularly for the case when the catalyst is present.

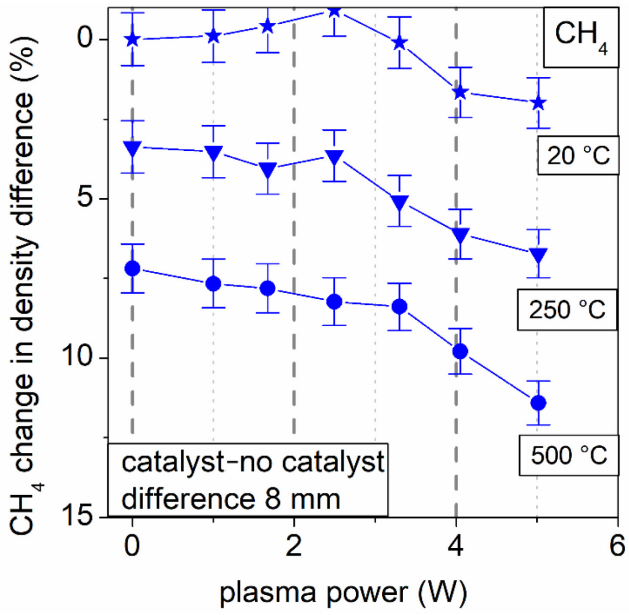

Figure 5: Difference between catalyst and no catalyst for percentage reduction compared to initial methane density for 500, 250, 20 °C temperatures at 8 mm distances.

The difference between the methane reduced for the plasma only case and the plasma with catalyst case is critical for understanding if there is a synergistic reaction occurring for the plasma catalyst system and is shown in Figure 5. We can see that the difference between these systems increases significantly with increasing temperature. This is due to the catalyst becoming more active with temperature and playing a more important role. However, at all temperatures we see an increase in the difference between the catalyst and no catalyst cases with increasing plasma power which indicates that the plasma power is playing an important role here. It is important to note that we get a notable difference with increasing plasma power at room temperature as well which indicates that we start to decompose the CH_4 molecules even though no thermal catalysis occurs here.

3.1.2 CO

The first of the species to be discussed is CO which shows a series of peaks from 2220 to 2060 cm^{-1} in the form of two separate wide bands.[30] These spectral features are only seen with plasma treatment at sufficiently high power.

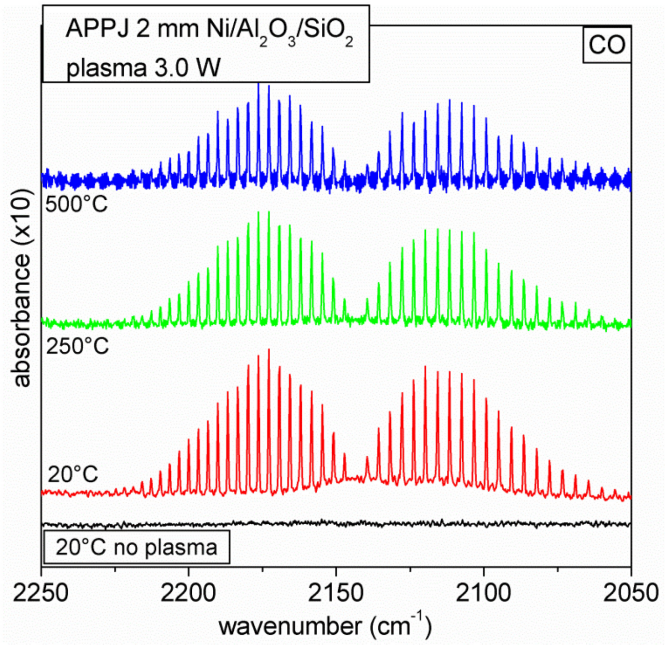

Figure 6: CO spectra for 3 W plasma power case, and catalyst temperatures of 20, 250, and 500 °C, respectively. The sequence of individual peaks is shown and used for CO density calculation.

The calculation for the density of the CO was done by using the cross section for 20 individual peaks, 10 from the center of each of the two hump shapes which correspond to the strongest signals from the CO in the gas phase. The specific peak positions are located at 2090.6, 2094.9, 2099.0, 2103.3, 2107.4, 2111.5, 2115.6, 2119.7, 2123.8, 2127.7, 2154.9, 2161.9, 2165.5, 2169.2, 2172.8, 2176.4, 2179.8, 2183.4, 2186.8, 2190.1 cm^{-1}. Each of these individual peaks is highlighted in the spectrum shown in Figure 6. The density was then calculated form the average of these peaks.

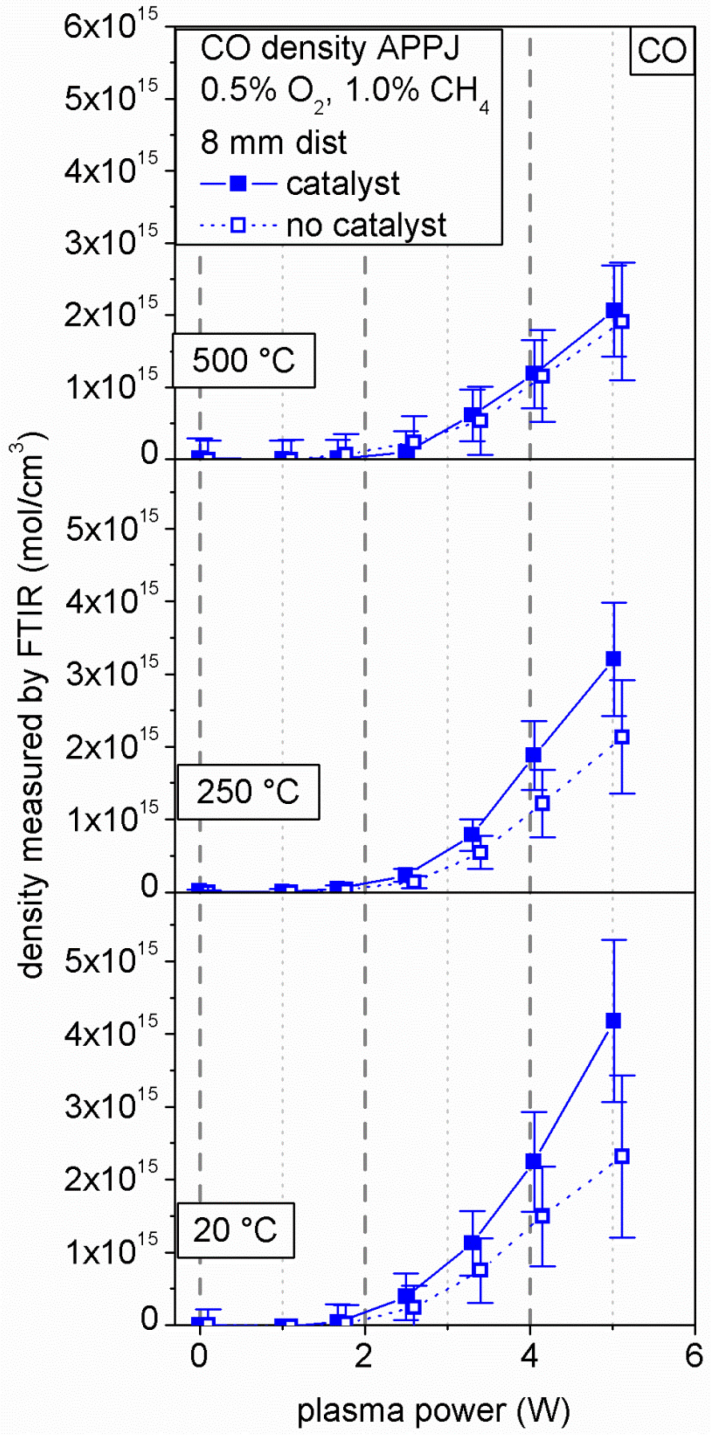

Figure 7: Carbon monoxide density for catalyst temperatures of 500, 250, 20 °C at 8 mm distances with catalyst and plasma only conditions.

The results of CO density calculation are shown in Figure 7 for the same conditions and Figure 4. From this data we can see that the density of CO decreases with increasing temperature. In addition, at the highest temperature the difference between the catalyst and no catalyst cases almost completely disappears suggesting that for this case most of the CO produced is coming from the plasma conversion of methane. It is also important to note that there is essentially zero CO production below 2.5 W plasma power for any conditions suggesting that a certain level of plasma density is required for this reaction pathway to occur.

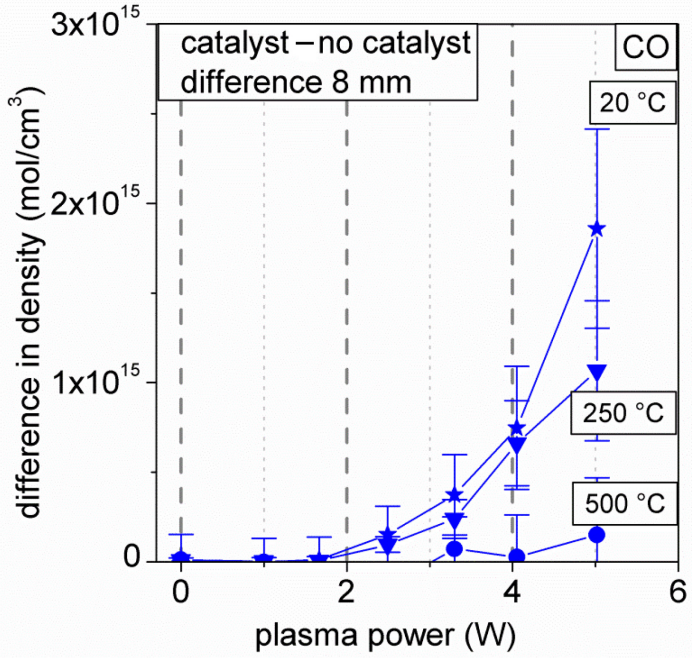

Figure 8: Difference of CO density for catalyst and no catalyst for 500, 250, 20 °C catalyst temperatures at 8 mm distances.

For the difference plot between the catalyst and no catalyst cases we can see that the difference in CO density shows the opposite trend from methane (see Figure 8). As temperature increases there is significantly less difference between these cases down to almost no difference at 500 °C. This suggests that the plasma is capable of stimulating the catalyst to produce CO species at a lower temperature but at higher catalyst temperature all the CO species seen are from plasma conversion only. It is also possible that the plasma produced CO species undergo further reactions at higher catalyst temperature, e.g. conversion of CO to CO_2 by reaction with oxygen or water vapor. The water shift reaction, shown in equation 5, requires 2.85 kJ/mol energy which is easily supplied by the process at higher temperatures. This would lead to a decrease in CO and H_2O at higher temperatures while seeing an increase in CO_2.

3.1.3 CO_2

Another species that clearly forms from this catalysis reaction is CO_2 which is differentiated from atmospheric CO_2 by having a nitrogen purge around the gas cell to reduce the influence of atmospheric CO_2 from our measurement. The CO_2 gives rise to a spectrum with peaks from 2380 to 2300 cm^{-1} in the form of two distinct groups of IR bands within this spectrum similar to the CO spectrum (Figure 9).[30] We see from this data that generally the CO_2 density increases as temperature increases.

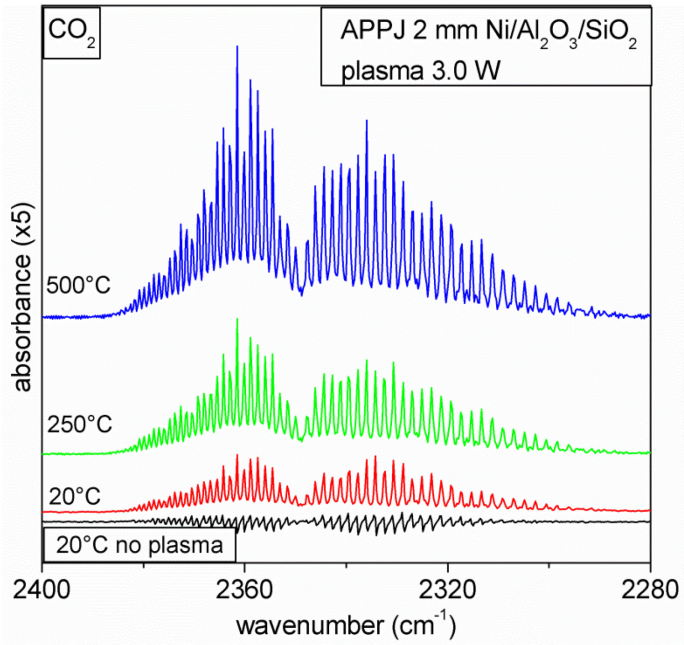

Figure 9: CO_2 spectrum for no plasma/3 W plasma and catalyst temperature of 20, 250, and 500 °C showing the individual peaks of CO_2 from which CO_2 density is calculated.

The carbon dioxide calculation was done using 48 peaks from the CO_2 spectrum, 24 from each of the two distinct groups of bands, similar to how CO was calculated. The specific peaks range from 2308.9 to 2380.8 cm^{-1} with approximately 1.5 cm^{-1} between each peak and are shown in detail in Figure 9. For this calculation it was assumed that we were able to remove most of the CO_2 from the ambient air around the measurement cell through an N_2 purge though there may be some slight residual CO_2 signal. The signal was checked by monitoring the CO_2 peak area while flowing the N_2 gas until the CO_2 was no longer reduced and then the background was taken for these measurements.

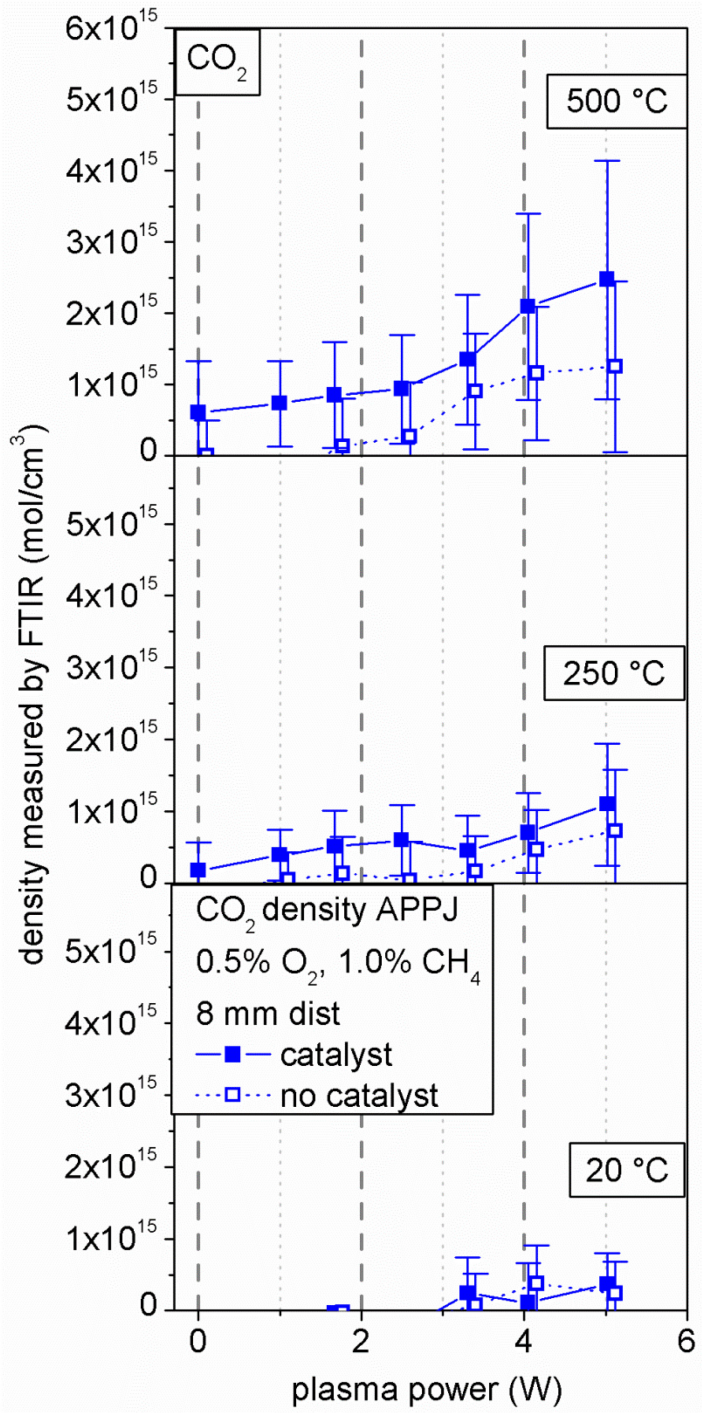

Figure 10: Carbon dioxide density for catalyst temperatures of 500, 250, 20 °C at 8 mm distances with plasma/catalyst and plasma only conditions, respectively.

The density calculation results for CO_2 are shown in Figure 10 and cover the same treatment conditions as Figure 4. For CO_2 we see primarily the opposite trend of the CO behavior, which is that the amount of CO_2 increases with catalyst temperature and that plasma power plays very little role in the CO_2 production. The only conditions we get any measureable CO_2 produced with the plasma is at 500 °C, with a plasma power of above 4 W and even here it is fairly small (less than 10^{15} cm^{-3}) when compared with the thermal catalyst case.

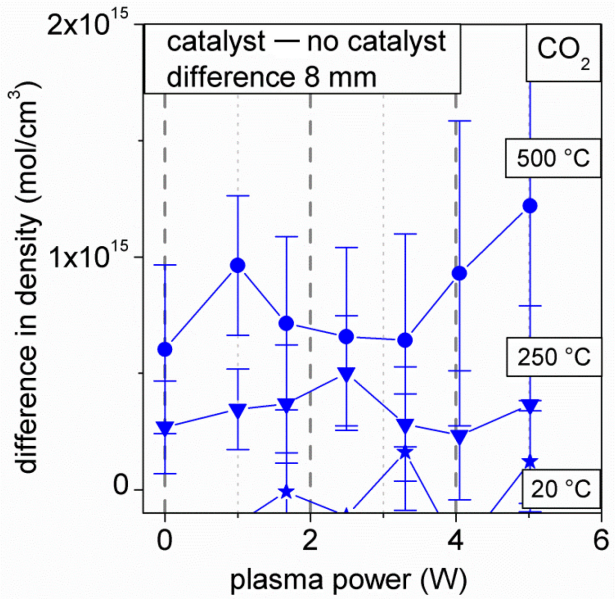

Figure 11: Difference between catalyst and no catalyst for CO_2 density for catalyst temperatures of 500, 250, 20 °C at 8 mm distances.

The difference plot, shown in Figure 11, between the catalyst and no catalyst cases shows a slight increase with plasma power overall but generally seems dependent more on the temperature of the catalyst. With increasing catalyst temperature we see an increased CO_2 production when the plasma is used in conjunction with the catalyst. The

measurements suggest that neither the catalyst nor the plasma produces CO_2 at low temperature but once the catalyst is activated at high temperature it is able to efficiently use plasma produced species to convert methane into CO_2.

3.1.4 H_2O

The final spectral features that we clearly see in the gas phase are from H_2O in the gas phase. Again, due to the presence of atmospheric H_2O, a nitrogen purge was used to reduce any influence from the local environmental air. This involved also to take a spectrum prior to the start of experiments to ensure that H_2O was stable. The spectral features are present in two different regions and consist of numerous small individual peaks throughout these two regions without the presence of the other species. The first of these spectral ranges is from 1800 to 1400 cm^{-1} with a small gap at the center around the 1600 cm^{-1} region and corresponds to the bending of the O-H bonds. The second spectrum is in the region from 3950 to 3550 cm^{-1} and corresponds to the stretching of the O-H bonds.

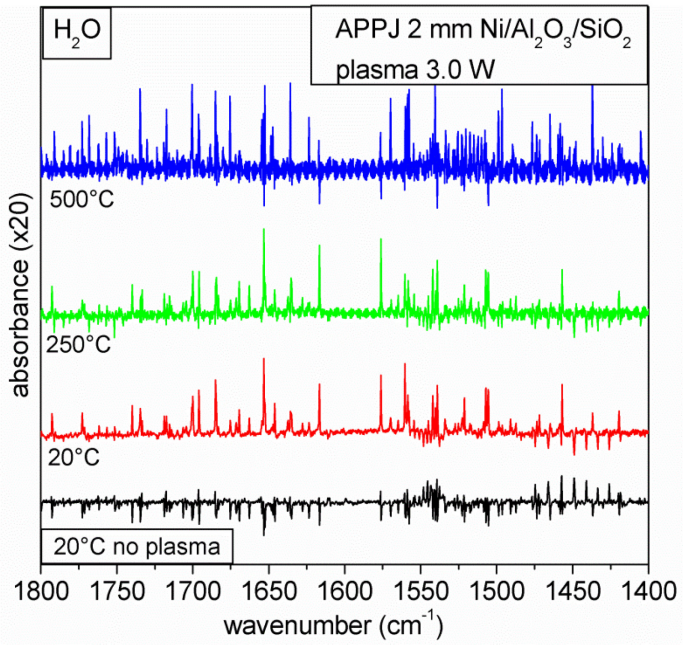

Figure 12: H_2O spectral features for 3 W plasma case, catalyst temperature of 20, 250, and 500 °C consisting of numerous individual peaks and used for obtaining H_2O density.

Compared to CO_2 and CO, the H_2O density calculation was the most difficult to perform accurately due to the non-structured nature of the IR peaks related to H_2O in the studied IR range. For this density calculation we selected the most distinct 11 peaks. The specific peaks are taken at 1455.8, 1505.9, 1538.0, 1557.6, 1575.2, 1615.7, 1652.3, 1683.9, 1699.1, 1716.4, 1733.5 cm^{-1} wavenumber. However, the small cross section of these peaks results in large errors. As seen in Figure 12 all the peaks aside from the few with the highest intensity are subject to a significant amount of noise and therefore difficult to use in a consistent density calculation. In conjunction with the fact that there is water vapor presenting in the atmosphere and on the wall of the measurement setup it was difficult to get an accurate measurement of H_2O. Therefore, the error associated with

these density measurements is fairly large. However, there are still some trends which stand out from the data collected.

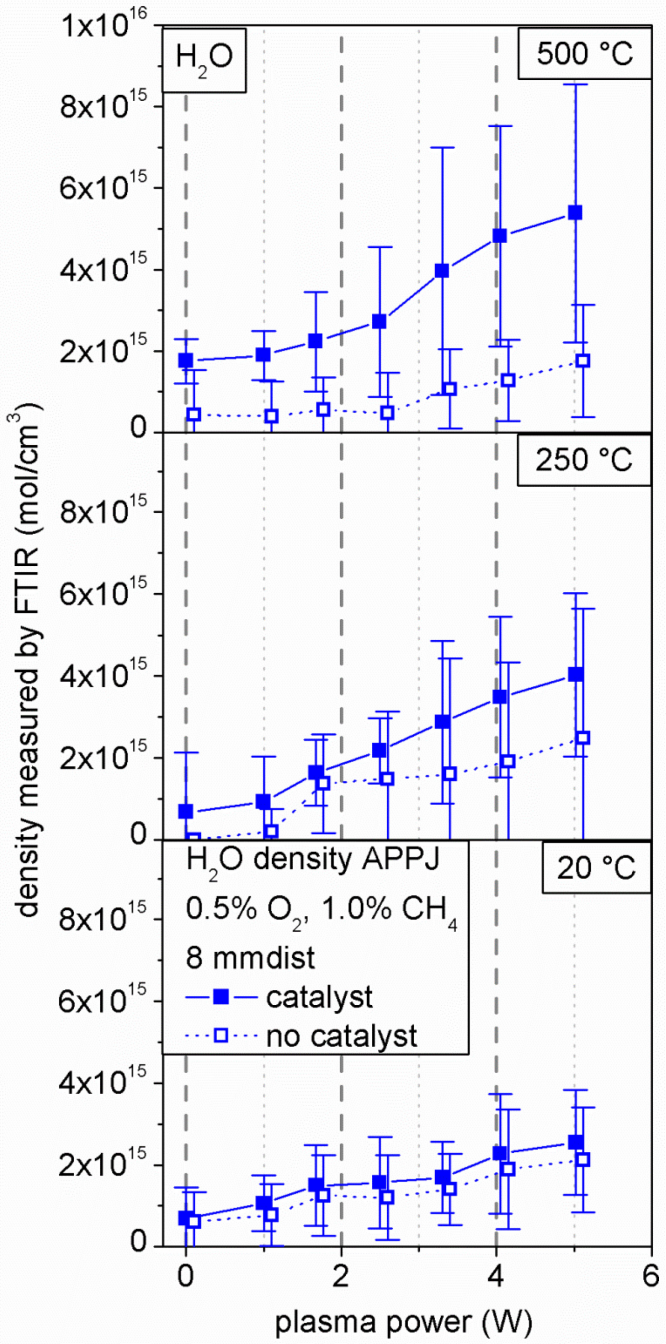

Figure 13: Water density for catalyst temperatures of 500, 250, 20 °C at 8 mm distance for plasma only and plasma/catalyst conditions.

The calculated densities of H_2O are shown in Figure 13 with same experimental conditions as shown in Figure 4. In general, the water density shows an increase with both increasing catalysis temperature and increasing plasma power. At 20 °C there is very little difference between the cases with and without catalyst present. This suggests that most of the H_2O production is from the plasma activated conversion. However, the amount of H_2O produced without catalyst present stays fairly constant over the range of temperatures so it is clear the catalyst starts to play a role as its temperature increases.

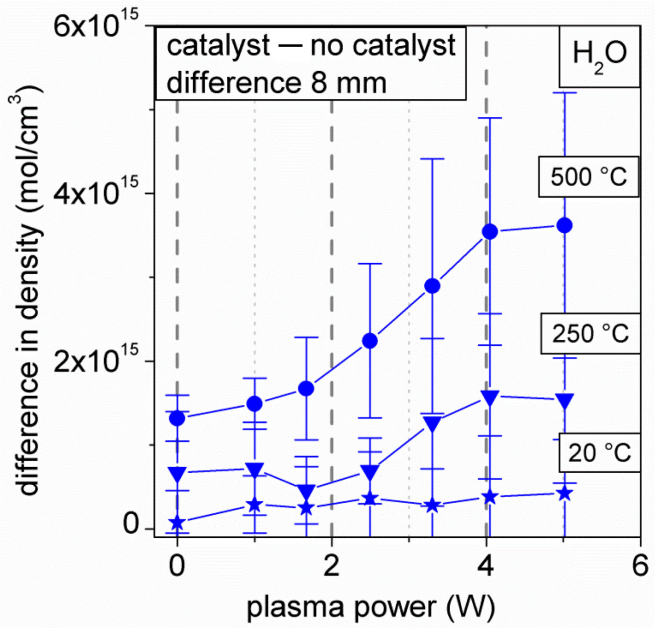

Figure 14: Difference between catalyst and no catalyst for H_2O density for catalysis temperatures of 500, 250, 20 °C at 8 mm distance.

The difference plot shown in Figure 14 between the catalyst and no catalyst cases looks initially to be very similar to the CO_2 species. However, we can clearly see that the difference scales significantly more with increasing plasma power for this species, especially at higher temperature. It seems that the plasma alone is able to produce H_2O

species but that the catalyst significantly increases this amount as it becomes active at higher temperatures. Indeed, once the catalyst is active it seems that a plasma-catalyst synergistic effect becomes observable for H_2O production. Additionally, we can see that the magnitude of the water produced scales up to 6 x 10^15 cm^{-3} which is a bit higher than that of the CO_2 density produced. It also appears that we get a bit of a plateau effect as we increase plasma power so that above a certain point the water density is no long increasing significantly.

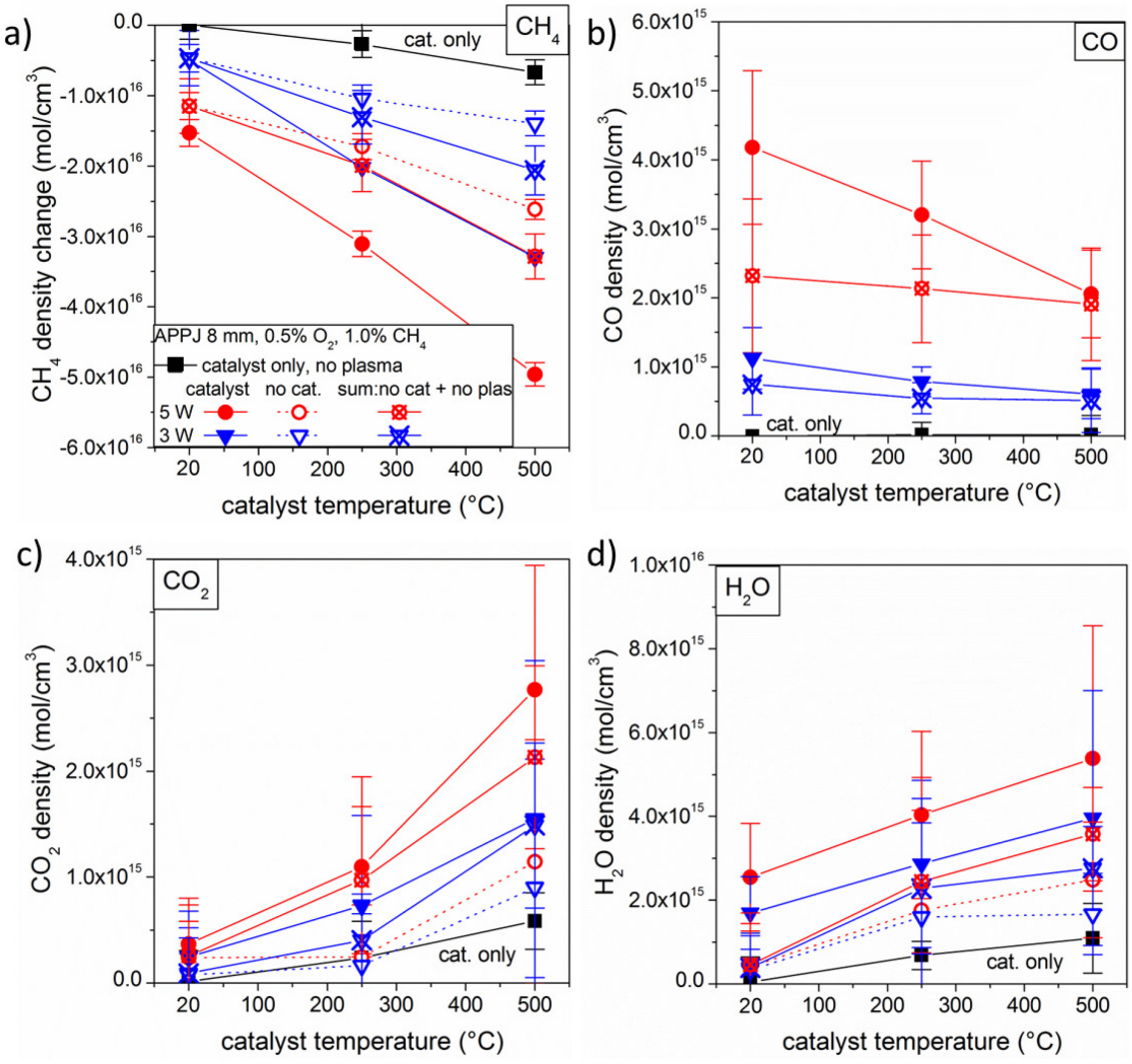

Figure 15: Comparison of various densities for two plasma powers for over a range of temperatures for a) CH_4, b) CO, c) CO_2, and d) H_2O measured gas phase species. Catalyst

alone without plasma present is shown by black squares. Plasma exposures with catalyst present are shown by solid filled markers and plasma exposures without catalyst are shown by hollow markers. The summation of the catalyst only and plasma without catalyst cases is shown by X filled markers.

A summary of all plasma conditions plotted vs catalyst temperature and compared to experiments using thermal catalysis only are shown in Figure 15. CH_4, CO, CO_2, and H_2O are shown in Figure 15 a), b), c), and d), respectively. For methane reduction we can see from Figure 15 a) that the catalyst alone is the least effective conversion at all temperatures, followed by the plasma alone. The combination of both catalyst and plasma gives the largest reduction. Indeed, the catalyst only and the plasma only added together are shown to be less than the plasma catalyst case for both plasma powers and at all temperatures. We see that the actual methane reduction is a factor of 1.51 larger at 500 °C and 1.33 larger for 20 °C for the plasma catalyst system compared to the sum of the catalyst and plasma only effects. This indicates synergy of catalyst-plasma system, although it is modest. There is also a clear difference in the slope of the methane reduction with respect to temperature.

The CO density shown in Figure 15 b) shows a reduction in CO density with increasing temperature, opposite the trend of the CO_2 and H_2O species. However, the dominant CO production seems to occur with higher plasma power. We see that the plasma alone case at 5 W is higher than the plasma/catalyst case for 3 W power dissipation. For catalyst alone without plasma present there is little if any CO produced at any temperature at or below 500 °C seen in this work. Therefore, without the plasma it seems that all of the catalyst behavior in this temperature range facilitates the production

of CO_2 and H_2O over CO. The sum of the catalyst only and plasma only cases is directly overlapping with the plasma only case and clearly demonstrates the increased CO production behavior of the plasma catalyst system above the sum of each parts alone. For 20 °C we see a 1.81 factor increase of the CO production with the plasma catalyst system over the sum of the plasma and catalyst effects along, though this falls off to a 1.07 at 500 °C which suggesting almost no synergistic production of CO at higher temperatures.

Figure 15 c) shows in detail the CO_2 peak signal seen for all experimental cases. Here we see the very sharply increasing behavior with increasing temperature for the CO_2 peak. This occurs regardless of plasma conditions, though it is enhanced by having the plasma active as well. The catalyst alone and the plasma alone cases here produce similar amounts of CO_2 across the plasma power and distance conditions shown here. The sum of the catalyst only and plasma only cases for CO_2 production is only very slightly lower than the experimental plasma catalyst case. The amount of synergy of CO_2 production shows a 1.42 factor increase at 20 °C, a 1.13 increase at 250 °C, and a 1.30 factor increase at 500 °C. When we look at CO and CO_2 together we see that CO density falls off from approximately 4 x 10^15 cm^{-3} density at room temperature down to about 2 x 10^15 cm^{-3} at 500 °C. In contrast to this, CO_2 production starts at 0.5 x 10^15 cm^{-3} at room temperature and increases up to 3 x 10^15 cm^{-3} maximum. This does suggest that the total density of CO + CO_2 remains close to 5 x 10^15 cm^{-3} for all the plasma catalyst conditions. This may provide some further evidence for conversion of CO to CO_2 in the presence of this plasma catalyst reaction at higher temperatures.

Figure 15 d) shows the H_2O peak behavior which also scales with temperature but still shows activity from the plasma treatment as well. This is clear from the nearly zero

water vapor produced by the catalyst alone at room temperature but the significant increase in H_2O signal with the addition of the plasma treatment at this temperature. There is still a clear enhancement of H_2O species produced as well for the plasma catalyst experimental case over the sum of the catalyst alone and plasma alone cases. Generally, it seems that these enhancements over the sums occur more significantly at lower temperatures. The enhancement factor is approximately 1.5-1.7 over the temperature range investigated here. This seems to be because at these temperatures the catalyst would have no affect alone, but the plasma produced species may be helping to activate the catalyst.

A brief look at the balance of the carbon in the system gives some insight into the amount of carbon converted to oxides vs the carbon deposited or converted to species not measured by FTIR. For the plasma and catalyst system at 8 mm 5 W plasma conditions we see the amount of carbon reduction in the system starts at about 3 times the amount of carbon converted to CO and CO_2. This amount then increases in an approximate linear fashion to about 10 times as the temperature is increased from room temperature up to 500 °C. For the same plasma conditions without catalyst present we see approximately the same different in carbon at room temperature but this difference only increases to about 7 times more methane carbon reduction at 500 °C. For catalyst alone, we see no effect at room temperature but for both 250 and 500 °C conditions we see approximately 11 times more carbon reduction than conversion to CO_x species. It is likely that for this case a significant amount of carbon is being deposited onto the catalyst surface. It is expected that the plasma treatment likely reduces some of this deposited carbon which could lead to more of the species converted to CO_x species for these cases. When

compared to the plasma treatment at 2 mm 3 W plasma conditions we see a similar trend. We see that for the plasma and catalyst case the amount of methane reduction starts at 4 times the CO_x species production and increases with increasing temperature up to 11 times. Additionally, we see a smaller increase with temperature for the case without catalyst which increases from 4 times up to about 9 times increase for methane reduction. This is very similar to the 5 W case though we see a slight trend toward more CO_x species compared to methane reduction for higher power plasma cases.

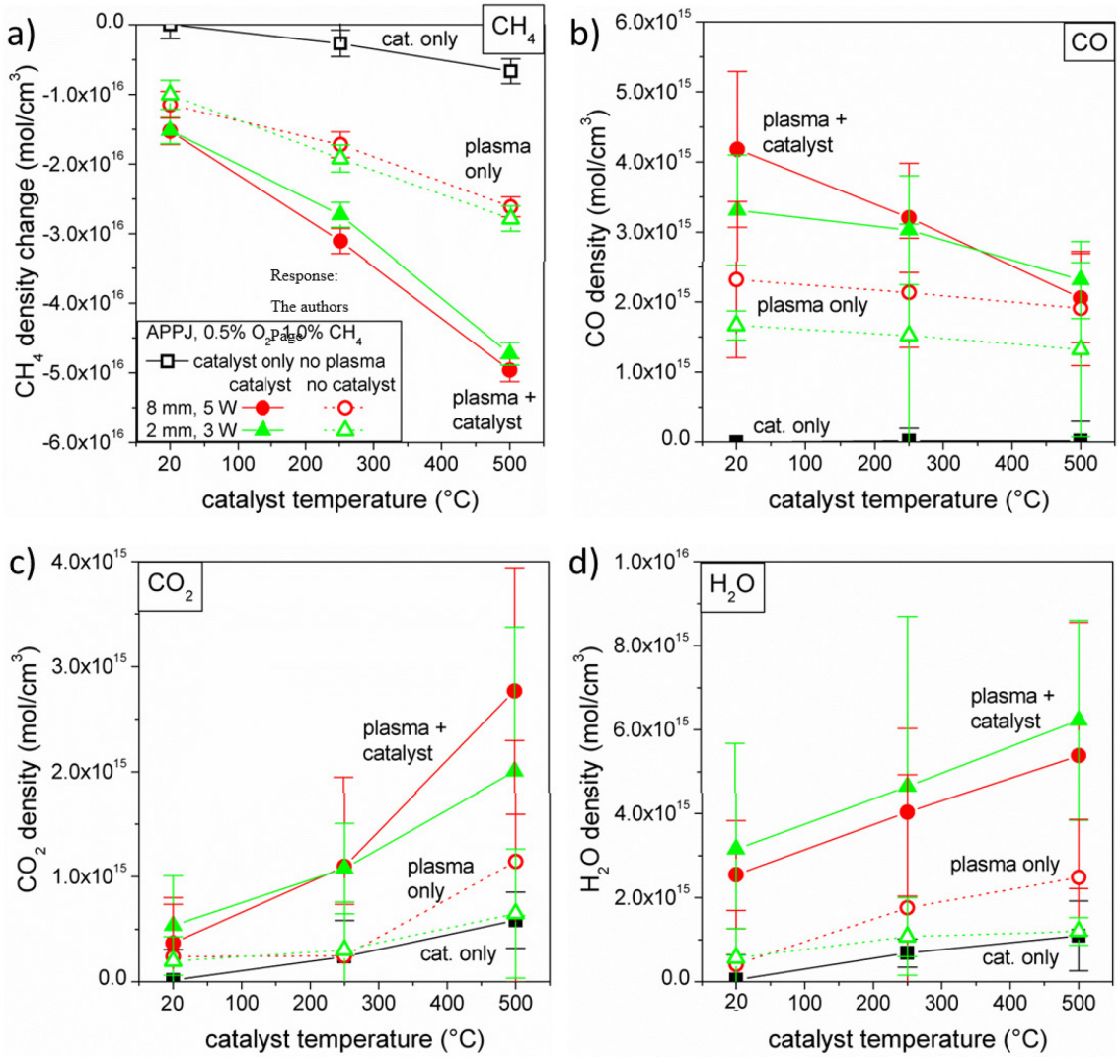

Figure 16: Comparison of various densities for two plasma distances for catalyst/no catalyst, and catalyst alone over a range of temperatures for a) CH_4, b) CO, c) CO_2, and d) H_2O.

Figure 16 highlights the difference between the 2 mm 3 W plasma case and the 8 mm 5 W plasma cases. For these conditions, the distance between the catalyst and the tip of the plasma plume is nearly identical, just barely above the top of the catalyst material. Under these conditions, we see in general that the methane conversion results and products produced are very similar. The main difference is a very slight reduction in the amount of methane conversion and products produced for the 2 mm 3 W case compared with the 8 mm 5 W case. However, this is not completely consistent for the H_2O spectrum, and overall these results are very similar for the same plasma plume to catalyst distance regardless of plasma power.

3.2 DRIFTS Measurement Results

The surface measurements were performed using the same plasma setup and same experimental conditions with the DRIFTs cell integrated into the FTIR system so the IR beam can be used to monitor the surface of the catalyst. Therefore, these measurements could not be done simultaneously to the gas phase measurements. However, these measurements are done *in situ* with a time resolution of approximately one minute and therefore we can monitor changes to the surface as they occur. Figure 17 shows examples of DRIFTs spectra taken *in situ* showing the surface prior to heating, after heating to 500 °C, during plasma treatment at this temperature, and then after plasma treatment has

stopped and the reaction chamber has been flushed with nitrogen gas to remove all gas phase species. This experiment distinguishes the changes that are due to IR light scattered from the solid surface and absorption of the IR light as it travels through the gas environment of the high temperature dome. Since pristine catalyst was used as the background of all DRIFTs spectra, the peaks that are in the negative direction of absorbance indicate that there is a loss of the species that was previously causing the IR light to be absorbed in that wavelength range. We can see from this experiment that the CO_2 peak and the two narrow CH_4 peaks are from IR light absorbed in the gas phase. However, there are several other interesting changes to the catalyst surface that occur and are stable after the plasma treatment has stopped and the local gas removed from the catalyst.

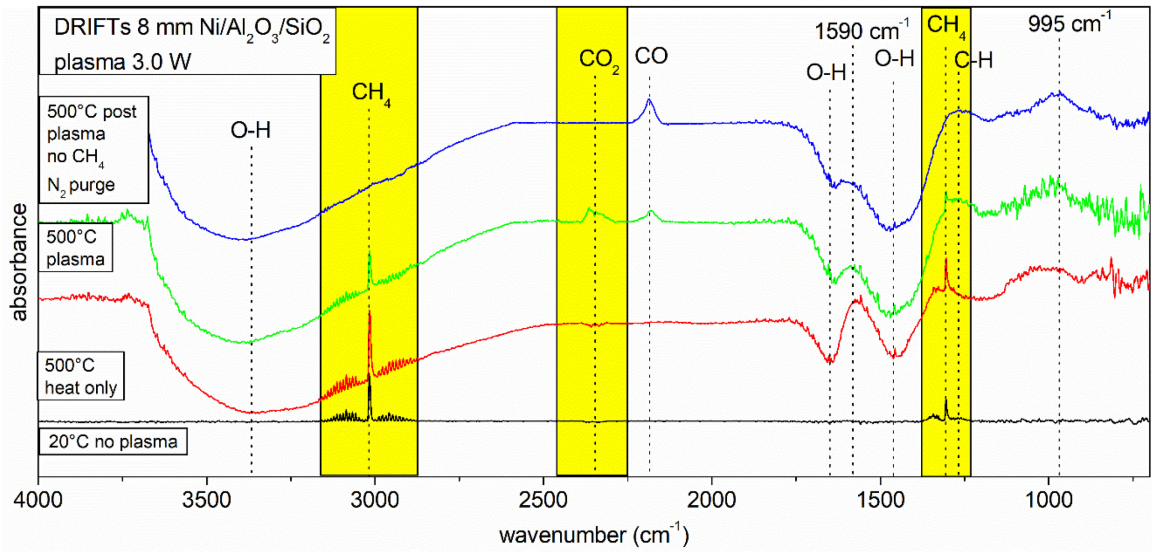

Figure 17: *In situ* DRIFTs at 8 mm distance with heating only to 500 °C, plasma treatment of 3 watts at 500 °C taken with 4 cm^{-1} wavenumber resolution with plasma on and then at 500 °C after extinguishing plasma and purging the reaction chamber with nitrogen gas.

The CH_4 peaks around 3050 cm^{-1} seen here are from the gas phase and correspond to the same peaks seen from the previous spectrum in Figure 2 with a much smaller magnitude due to the significantly smaller path length of the IR beam in the DRIFTs cell. The CO_2 as well is similar to the spectrum seen in the gas phase section 3.1.3, and due to the sharpness of the peaks which suggests it is not a surface bound species. It should be noted that the CO_2 seen here may be from part of the reactions occurring since we know from the previous data that CO_2 production is maximized at increased temperatures and we see it becoming the strongest for the 500 °C plasma case. As mentioned from the section on gas phase (section 3.1), CO_2 contribution from the background gas was reduced as much as possible but may still play a role in the measurements as well.

There are also several spectral features which seem to be caused primarily by the increased temperature of the catalyst surface. The background of the spectrum was taken at room temperature untreated catalyst which likely still contains moisture from the local environment to show the raw effect of the plasma treatments without any data processing. The most pronounced of these is loss in intensity of the O-H regions at ~3400 cm^{-1}, 1650 cm^{-1}, and 1450 cm^{-1}. These features are clearly related to a surface bound species due to the large broad shape of the spectral features whereas the water vapor FTIR peaks show numerous small sharp spikes in these regions. This loss might be due to the removal of adsorbed water on the catalyst surface from the exposure to the atmosphere prior to the experiment. These features are weak after having dry gas flow, such as Ar, over the catalyst sample for long periods of time. They also appear significantly for both plasma treatment and heating of the catalyst sample. However, heating pretreatments to ~100 °C

for long periods of time could never fully remove water from the catalyst surface as compared to plasma treatment. In other words, there is water molecules adsorbed on the surface of catalyst samples that stay on the surface to very high temperatures but could be then removed by plasma treatments. A similar observation has been reported in previous work involving catalysis, for instance when using DRIFTs to investigate a Ni/TiO_2 catalyst, in which only a 26% reduction in OH groups by heating to 150 °C was seen.[32]

The other spectral feature that appears after heating only and is stable on the surface is a spectral feature centered at ~995 cm^{-1} which is marked in Figure 17. For this very broad feature several explanations are possible, including NiO formation as the Ni is oxidized by the oxygen from the environment and from the catalyst support materials SiO_2 and Al_2O_3. This spectral feature will be discussed further in the discussion section 4.2.1 of this paper.

Plasma treatment alone appears to cause the appearance of a surface bond CO on the catalyst material. This feature position is primarily at 2190 cm^{-1} though there is some shift (~10 cm^{-1}) depending on the conditions of the plasma treatment and catalyst temperature. We can see that the CO shown here is stable since it is still present after plasma treatment and flushing the gas away with nitrogen. Additionally, this feature is broader and has more absorption than the CH_4 and CO_2 peaks and compared to the gas phase data.

The final spectral feature that displays an interesting behavior is the feature centered at 1590 cm^{-1} which is marked on Figure 17. This feature is located in between the two O-H features which show significant reduction from heating and plasma

treatment. However, this feature is stable when heating alone up to a certain temperature on the magnitude of ~500 °C where it does start to decrease, but then shows an increase at weaker plasma treatments and a decrease at more significant plasma power treatments. While it is difficult to determine what species give rise to this feature, one possibility is a C-O-O based species. This spectral feature will be discussed further in the discussion section of the paper under the surface results.

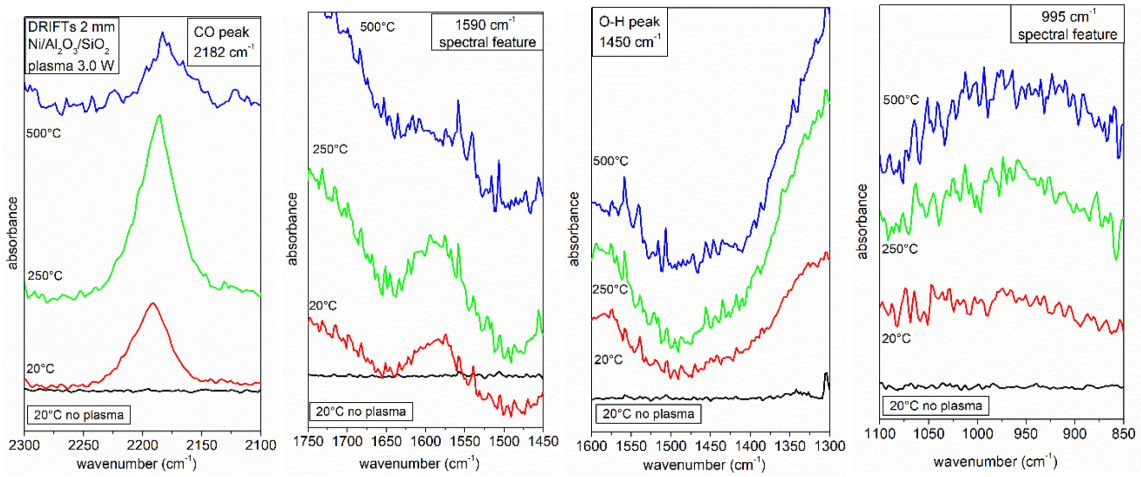

Figure 18: DRIFTs spectrum for no plasma at 20 °C and the 2 mm 3 W plasma case at 20, 250, and 500 °C showing the spectral feature evolution focused on 4 narrow spectrum ranges.

Figure 18 shows the raw spectrum of the 2 mm 3 W plasma condition over various temperatures compared with the case prior to plasma exposure at 20 °C. The behavior of four of these critical spectrum areas which have been shown to be sensitive to plasma treatment or heating are described in this Figure 18. The first of these is the CO spectra, which is shown in Figure 18 in the first panel in the range of ~2190 cm^{-1}. The

other spectral feature that behaves in a similar manner at 1590 cm^{-1} and the raw spectrum of this feature for 2 mm 3 W plasma conditions over various temperatures is shown in Figure 18 in the second panel. Both of these two features shown some formation with plasma treatment that is then removed once this plasma treatment reaches a certain power level or substrate temperature. Two additional features of interest are the O-H features and the 995 cm^{-1} spectral feature both of which respond to temperature alone and plasma treatment as well. The behavior of the O-H feature at 1450 cm^{-1} raw spectrum for 2 mm 3 W plasma conditions is shown in Figure 18 in the third panel and behaves similarly to the other O-H features. The behavior of the 995 cm^{-1} spectral feature for 2 mm 3 W case is over various temperatures is shown in Figure 18 in the fourth panel.

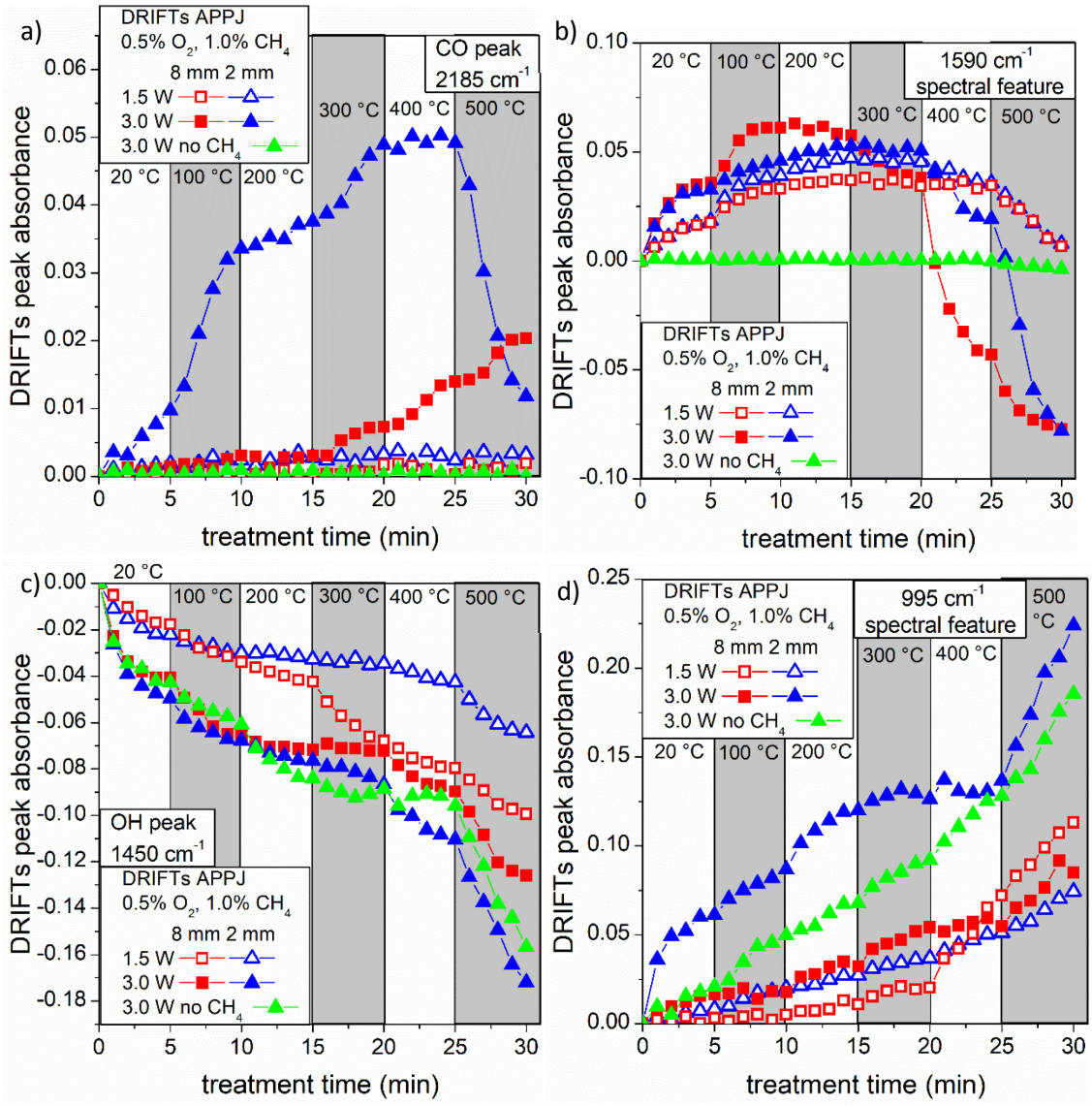

Figure 19: *In situ* DRIFTs peak absorbance of a) CO feature, b) 1590 cm^{-1} spectral feature, c) OH feature, and d) 995 cm^{-1} spectral feature over time for 1.5 and 3 W at 2 and 8 mm.

The behavior of the CO formation over temperature, time, distance, and power changes is shown fully in Figure 19 a). We see that at the weaker plasma treatment

conditions of 1.5 W, no surface CO is formed at all. This corresponds to the gas phase data as well where we see no CO formed for any temperature or conditions if the plasma power is below 2.5 W. For a plasma power of 3 W and 8 mm distance we see that a CO feature appears on the surface once we reach a certain temperature of above 200 °C and then the absorbance peak increases with increasing temperature. However, at the 3 W and 2 mm plasma case we see immediate CO production on the surface at the lowest temperature, the CO feature then initially increases with temperature before being almost completely removed at the highest temperature measured here (500 °C). We also see that the drop off of the CO peak at 500 °C occurs very quickly upon reaching this temperature before stabilizing at a much lower critical value of CO. This result was confirmed several times by testing the removal of CO by studying higher catalyst temperatures and plasma powers after it had been formed. However, removal of the CO was not possible by increasing temperature alone even up to 700 °C; only when there is additional plasma interacting with the catalyst surface do we see removal of CO at this high energy case. Additionally, we see that if we treat the catalyst with plasma without any CH_4 present at 2 mm distance 3 W we do not see any CO production for any temperature. This supports that the CO bonded to the surface is coming from a reaction of the methane with the oxygen present.

The extracted data for the behavior of the 1590 cm^{-1} spectral feature over a range of temperatures at different distances and powers is shown in Figure 19 b). This feature initially shows a slight increase with all plasma treatments at lower temperatures and then above a certain temperature the peak absorbance for this feature drops significantly, particularly for the higher power plasma treatment. The shift from increasing to

decreasing seems to occur at about 200-300 °C for the 1.5 W plasma power cases and the 8 mm 3 W plasma case but the shift occurs a lower temperature for the 2 mm 3 W plasma power case. This is likely due to the increased plasma energy and reactive species reaching the surface for this case. Again, it seems like the plasma initially causes this species to be formed on the surface before reaching a sufficient energy to then remove it. We see very little impact of the plasma when there is no CH_4 present except once reaching 500 °C where we see a very small reduction in the feature. Similar to the CO feature, this likely means that the production of this feature is tied to the carbon from the methane being decomposed.

The extracted behavior of the O-H spectral feature over plasma distance and power is shown in Figure 19 c). In general, the higher the temperature the more this feature is decreased signaling more water removed from the catalyst surface. Additionally, increasing plasma power seems to increase the loss of signal for the O-H feature as well. In contrast to CO and the 1590 cm^{-1} spectral feature, O-H seems to behave similarly regardless of the presence of the CH_4 in the gas phase.

The spectral feature at 995 cm^{-1} is the other feature that behaves similarly to the O-H spectra and is shown in Figure 19 d) over plasma powers, distances, and temperatures. For most experimental conditions this feature seems only to scale with increasing temperature more than plasma power which makes sense since we see this feature form from only heating the catalyst without plasma. However, the 2 mm 3 W case does show a significantly higher absorption from this feature. This spectral feature also seems to behave similarly regardless of the presence of the CH_4 in the gas phase.

4. Discussion

4.1 Gas Phase Results

The balance between methane decomposition and production of CO, CO_2, and H_2O depends on numerous factors, more than what can be explored in this work alone. The contribution of the plasma alone is shown for the gas phase results but this becomes complicated once the catalyst is added in. Generally, we see significantly increasing plasma effects as the plasma power increases and the distance decreases, likely due to the travel of the reactive species from the source to the catalyst material. For instance, CO shows a significant increase from having the catalyst and plasma present at low temperature but then drops off at higher temperature. This may be due to the initial reactions in the plasma favor the formation of CO whereas at higher temperatures the reactions change to favor CO_2 production. It is likely that the higher catalyst temperatures favor the oxidation of CO by oxygen sources in the gas phase which is why the CO production drops off significantly. There is evidence of this with how the CO_2 increases significantly with temperature, much more so than H_2O. This could be because H_2O is a reactant and CO_2 is a product of the CO oxidation reaction. The increase of CO from adding the catalyst and plasma together demonstrates clearly that while the plasma is critical for CO production, the catalyst materials also helped promote the production CO. It should be noted in this discussion that the most ideal case of studying catalytic effect using a proxy material which is similar to the support material for the catalyst but without nickel was not conducted in this work. However, we believe that the evidence of comparing plasma only, catalyst only, and the summation of these two cases with the plasma and catalyst at once provides compelling evidence for the catalytic enhancement

by plasma considering we take measures to keep the plasma the same for each of these cases.

There has been significant literature starting to look at oxidation of VOC compounds by plasma catalyst systems. Lu et al. study toluene removal by a dielectric barrier plasma source with iron catalyst and show a significant increase of toluene removal scaling with increasing plasma power in addition to doing some investigation into surface states post treatment.[33] This work breaks down the CO vs CO_2 yield for this system and show that CO yield increases significantly for increased plasma power over CO_2 yield. There have been several other publications looking at similar balanced of CO and CO_2 for VOC removal by plasma sources including work by Zhang et al.[34] for TiO_2 catalyst in a DBD source and Klett et al.[35] using a packed bed plasma reactor for removal of acetaldehyde.

4.2 Surface Results

4.2.1 Spectral Feature Assignment

The 995 cm^{-1} spectral feature shows significant changes of IR absorbance with temperature which could provide key insights to the activation of the catalyst surface. A possible candidate for this feature is formation of an oxide of nickel. The behavior of this feature moves opposite that of O-H which means that as water is removed from the surface this feature forms. This feature forms around the 300 °C point which is where previous experiments have shown oxidation to occur for thin Ni films. NiO when studied in the form of nanoparticles has shown a significant and fairly broad spectral feature form

around 1040 cm^{-1} which is very close the position of the feature seen in the current work.[36] A similar broad spectral feature from 930-960 cm^{-1} has also been seen in previous work on Ni catalysis, but was left unassigned as the authors were unsure of the exact species responsible.[32] More evidence for the NiO is that the feature forms around 300 °C-400 °C which is approximately the temperature at which Ni will oxidize with some oxygen present in the ambient air.[37] The other possibilities for this feature assignment seems to be a low end of the alkoxy C-O bonding which is typically from 1050-1150 cm^{-1} which is what would appear from a partially oxidized methane molecule where one H is abstracted. Another possibility is sp^2 C=C bonding such as an alkene molecule which shows absorption in the range of 985-1000 cm^{-1}.[38] However, this possibility is unlikely due to the oxidative environment caused by the oxygen containing plasma which produces species such as ozone that react at a very high rate with sp^2 carbon. Another possibility which is the reaction of water molecules with silicon on the support material to form Si-OH which has been seen in the literature as a spectral feature at ~775 cm^{-1}.[39] This reaction would occur generally at higher temperatures as the water molecules are broken down and the Si-O bonds are broken in the SiO_2 material from the catalyst support. If this feature is indeed NiO then not only this is consistent with the expectation that nickel will be oxidized at certain temperature, but also it implies that highly reactive oxygen species produced by the plasma jet such as atomic oxygen[40] would oxidize the nickel surface.

The most likely possibility for the 1590 cm^{-1} spectral feature is COO^- or carboxylate groups. This surface species would be an excellent candidate for removal and the formation of CO_2 in the gas phase. Based on the literature COO^- or carboxylate

groups can form in conjunction with metal ions and one of the strong features that is characteristic of COO^- in the IR range is at 1586 cm^{-1}.[41] Indeed, other work that investigates plasma catalyst interactions through DRIFTs have seen this same feature, though they used a different catalyst material and studied the decomposition of different gas species.[17,42,43]

4.2.2 Behavior of CO: Comparison of Gas Phase and Surface Related Data

One of the most interesting observations that can be made from this work come from comparing the gas phase results to the surface results on the catalyst material. Based on how CO bonds to other metal surfaces, it is likely that the $CO_{(s)}$ seen here is bonded to the metal surface by chemisorption. While we clearly see CO produced in the gas phase for all conditions above 2.5 watts, we do not see it absorbed on the surface for all these conditions. In fact, for greater distance plasma treatments we see that $CO_{(s)}$ is absorbed on the surface only after the temperature reaches 300 °C by which point the contribution of CO production from the catalyst seems to be greatly diminished. It is possible that the reason we see the difference between the temperature range for CO in the gas phase is that a certain point the surface becomes active enough to strongly bind the $CO_{(s)}$ to the surface allowing us to see it using DRIFTs even after the plasma treatment has ended. However, it is important to remember that $CO_{(s)}$ often reacts with surface oxygen to form CO_2 which is then desorbed from the catalyst surface.[44] Therefore as the temperature reaches 500 °C and the $CO_{(s)}$ starts to be removed from the surface by the plasma treatment, we may see a spike in CO_2 production and CO production. For the 2 mm 3 W

case we see that there is still a significant amount of CO produced in the gas phase for this condition, especially compared to the case for plasma only. This could be signal from $CO_{(s)}$ being removed from the surface by the plasma treatment as seen by the DRIFTs measurements. This relationship of species deposition on the catalyst surface will be investigated in further detail in future works. This further investigation will also focus on clarifying the impact of these deposited layers on catalytic behavior and discuss how this impacts catalyst regeneration.

The relationship between CO seen in the gas phase and the surface suggests an interesting interplay between plasma produced species and catalyst produced species. We clearly see at low temperature that there is a significant amount of CO in the gas phase when the plasma is present and that this in enhanced by having the catalyst present. At further distances we see that the catalyst surface is showing still increasing amounts of surface bound $CO_{(s)}$ nearing 500 °C. At these same conditions in the gas phase we see no difference between plasma with and without catalyst suggesting that the catalyst is acting as a sink for the species being created by the plasma at these higher temperatures. At the closer treatment distance, we see a significant drop off in the surface $CO_{(s)}$ at 500 °C. For this condition in the gas phase we see a significant increase in CO produced from having the catalyst added compared to plasma alone. This suggests that the CO that was bound to the surface previously now has enough energy to be removed from the surface explaining these two behaviors of CO seen.

A similar effect is seen with the spectral feature at 1590 cm^{-1}, which is assumed to be COO^- for this discussion, on the surface compared with CO_2 species in the gas phase. The CO_2 production seen in the gas phase increases significantly more from 250 to 500

°C than from 20 to 250 °C. Part of this increase may correspond to the removal of COO^- bonded to the surface of the catalyst. We initially see an increase in bonded COO^- until the temperature increases above 400 °C at which point we see a significant drop off. This reaction is further complicated however by the possible conversion of CO to CO_2 from available energy and oxygen in the reaction environment or on the catalyst surface.

CO production as a product from has been investigated for plasma methane decomposition with catalyst materials other than nickel before. Lee et al. (2015) used a DBD style plasma source with a Pd based catalyst and saw a similar behavior of CO production to this work.[45] They see a distinct reduction in CO production with increasing temperature after a small increase up to 100 °C. It also increases with increasing plasma power which is similar to what we see here in our work.

4.2.3 Changes in FTIR Frequency

There are several things that can cause a shift in the feature position in FTIR spectrum. One paper investigating various species that can absorb onto metal substrates shows that CO absorbed on the metal surface can shift to a lower wavenumber and this shift correlates to an increase in the surface coverage of the CO on the metal surface.[46] Another work looking at CO absorption on nickel surfaces states how CO feature position is a function of dipole-dipole interactions and is therefore dependent on the substrate temperature as well as surface coverage.[47] In general, a lower wavenumber indicates more weakly bonded CO to the surface, which when due to surface coverage is because there are more CO molecules competing for the same surface electrons to bond with.[48] However, in our case it seems that we may have a weaker bonding state due to the

increased surface energy since we simultaneously see a weakening DRIFTs CO signal which would mean less CO absorbed on the surface. It seems that for the CO production on the surface that below a certain plasma power there is simply no CO produced in the gas phase and therefore there is no CO to be bonded to the surface. However, once there is CO in the gas phase the surface must reach a certain energy state before CO can be bonded to the catalyst surface in a semi-permanent manner. Once this occurs there is then another energy threshold above this where the CO can then be removed from the surface via a combination of plasma and thermal energy.

There has been some significant effort on beginning to investigate the interactions between plasma and catalyst materials. Stere et al. (2015) has investigated a Ag/Al_2O_3 catalyst for the decomposition of toluene and n-octane with a plasma treatment directly onto the catalyst material using a helium based ring style plasma source.[17] They attribute the feature seen at 2165 cm^{-1} to cyanide absorption on the surface and a NCO species absorbed on the surface which has a feature at 2260 cm^{-1}, however they include NO into their feed gas which complicates their system compared to our work since they are trying to simulate diesel exhaust gas. There has been other work looking at the effect of nickel catalyst in conjunction with a plasma reactor but they primarily look at the species produced and do no measurements of the catalyst surface after the plasma treatments.[49,50,51,52]

5. Conclusions

We have demonstrated a new methodology for investigating how plasma species interact with catalyst surfaces in the catalytic conversion of chemical compounds. We can monitor the surface changes *in situ* and compare them directly to changes we see in the gas phase. For this work specifically the reduction in methane by a plasma and catalyst system was studied and the products of this reaction including CO, CO_2, and H_2O were measured. CO production in the gas phase seemed to be primarily due to the plasma interacting with the catalyst surface and only is significant above a plasma power of 2.5 W. CO_2 production is controlled primarily by the catalyst temperature and H_2O production seems to be a product of both catalyst and plasma. The nickel catalyst surface changes significantly from both heating and plasma exposure. A spectral feature at 995 cm^{-1} forms due to heating of the nickel alone though can be accelerated by plasma treatment and additionally heating. This feature could be due to NiO formation, but other possibilities have been discussed. Additionally, heating and plasma removes the water absorbed on the catalyst surface. A spectral feature at 1590 cm^{-1} forms which seems likely related to a carbon oxygen bonded species shows an initial increase with plasma treatment and then a significant decrease once above a certain temperature and plasma power. This feature is likely related to carboxylate groups on the surface which may be a precursor to CO_2 production. This behavior is also seen with the CO absorption on the surface of the catalyst though we see both the formation and reduction occur over the range of plasma conditions, though the initial formation is likely due to the production of CO in the gas phase. There are other connections between the gas phase and surface, for instance the formation of COO^- on the surface disappears as the temperature increases

above a certain point for which we see a significant increase in the amount of CO_2 that is produced in the gas phase.

6. Acknowledgements

The authors gratefully acknowledge financial support by the US Department of Energy (DE-SC0001939) and National Science Foundation (CBET-1703211). We also would like to thank C. Li, A. Pranda, K. Lin, L. Shafti, T. Dabrow, J. Jiang and Prof. P. J. Bruggeman for their helpful discussions and support of the project.

References

[1] E. C. Neyts, K. Ostrikov, M. K. Sunkara, and A. Bogaerts, Chemical Reviews 115 (24), 13408 (2015).

[2] J. C. Whitehead, Pure Appl Chem 82 (6), 1329 (2010).

[3] J. Christopher Whitehead, J. Phys. D: Appl. Phys. 49, 243001 (2016).

[4] H. H. Kim, Y. Teramoto, A. Ogata, H. Takagi, and T. Nanba, Plasma Chem Plasma P 36 (1), 45 (2016).

[5] C. E. Stere, W. Adress, R. Burch, S. Chansai, A. Goguet, W. G. Graham, and C. Hardacre, Abstracts of Papers of the American Chemical Society 247 (2014).

[6] S. Tang, J. Lin, and K. L. Tan, Surf Interface Anal 28 (1), 155 (1999).

[7] U. Zavyalova, P. Scholz, and B. Ondruschka, Appl Catal a-Gen 323, 226 (2007).

[8] X. Tu and J. C. Whitehead, Appl Catal B-Environ 125, 439 (2012).

[9] Q. H. Trinh and Y. S. Mok, Korean Journal of Chemical Engineering 33 (3), 735 (2016).

[10] B. Pietruszka, K. Anklam, and M. Heintze, Applied Catalysis a-General 261 (1), 19 (2004).

[11] E. C. Neyts and K. Ostrikov, Catal Today 256, 23 (2015).

[12] Y. F. Guo, D. Q. Ye, and K. F. Chen, J Environ Sci-China 18 (2), 276 (2006).

[13] S. Y. Shang, G. H. Liu, X. Y. Chai, X. M. Tao, X. Li, M. G. Bai, W. Chu, X. Y. Dai, Y. X. Zhao, and Y. X. Yin, Catal Today 148 (3-4), 268 (2009).

[14] H. J. Gallon, X. Tu, M. V. Twigg, and J. C. Whitehead, Applied Catalysis B-Environmental 106 (3-4), 616 (2011).

[15] X. Tu, H. J. Gallon, and J. C. Whitehead, Catalysis Today 211, 120 (2013).

[16] L. Wang, Y. Zhao, C. Y. Liu, W. M. Gong, and H. C. Guo, Chemical Communications 49 (36), 3787 (2013).

[17] C. E. Stere, W. Adress, R. Burch, S. Chansai, A. Goguet, W. G. Graham, and C. Hardacre, ACS Catal. 5 (2), 956 (2015).

[18] Zixian Jia, Xianjie Wang, Frederic Thevenet, and Antoine Rousseau, Plasma Processes and Polymers 14 (6), 1600114 (2017).

[19] Anthony Rodrigues, Jean-Michel Tatibouët, and Elodie Fourré, Plasma Chemistry and Plasma Processing 36 (4), 901 (2016).

[20] C. E. Stere, W. Adress, R. Burch, S. Chansai, A. Goguet, W. G. Graham, F. De Rosa, V. Palma, and C. Hardacre, ACS Catal. 4 (2), 666 (2014).

[21] H. M. Swaan, V. C. H. Kroll, G. A. Martin, and C. Mirodatos, Catal Today 21 (2-3), 571 (1994).

[22] E. Ruckenstein and Y. H. Hu, Appl Catal a-Gen 133 (1), 149 (1995).

[23] J. J. Guo, H. Lou, H. Zhao, D. F. Chai, and X. M. Zheng, Appl Catal a-Gen 273 (1-2), 75 (2004).

[24] M. C. J. Bradford and M. A. Vannice, Appl Catal a-Gen 142 (1), 73 (1996).

[25] K. Wende, P. Williams, J. Dalluge, W. Van Gaens, H. Aboubakr, J. Bischof, T. von Woedtke, S. M. Goyal, K. D. Weltmann, A. Bogaerts, K. Masur, and P. J. Bruggeman, Biointerphases 10 (2), 029518 (2015).

[26] W. Van Gaens, P. J. Bruggeman, and A. Bogaerts, New J Phys 16, 063054 (2014).

[27] S. Q. Zhang, W. van Gaens, B. van Gessel, S. Hofmann, E. van Veldhuizen, A. Bogaerts, and P. Bruggeman, J Phys D Appl Phys 46 (20), 205202 (2013).

[28] J. Y. Jeong, S. E. Babayan, V. J. Tu, J. Park, I. Henins, R. F. Hicks, and G. S. Selwyn, Plasma Sources Sci T 7 (3), 282 (1998).

[29] S. Hofmann, A. F. H. van Gessel, T. Verreycken, and P. Bruggeman, Plasma Sources Science & Technology 20 (6) (2011).
[30] Laurence S Rothman, Iouli E Gordon, Yury Babikov, Alain Barbe, D Chris Benner, Peter F Bernath, Manfred Birk, Luca Bizzocchi, Vincent Boudon, and Linda R Brown, Journal of Quantitative Spectroscopy and Radiative Transfer 130, 4 (2013).
[31] X. E. Verykios, Int J Hydrogen Energ 28 (10), 1045 (2003).
[32] M. C. J. Bradford and M. A. Vannice, Applied Catalysis a-General 142 (1), 97 (1996).
[33] M. J. Lu, R. Huang, J. L. Wu, M. L. Fu, L. M. Chen, and D. Q. Ye, Catal Today 242, 274 (2015).
[34] H. B. Zhang, K. Li, T. H. Sun, J. P. Jia, Z. Y. Lou, and L. L. Feng, Chem Eng J 241, 92 (2014).
[35] C. Klett, X. Duren, S. Tieng, S. Touchard, P. Jestin, K. Hassouni, and A. Vega-Gonzalez, J Hazard Mater 279, 356 (2014).
[36] A. S. Adekunle, J. A. O. Oyekunle, O. S. Oluwafemi, A. O. Joshua, W. O. Makinde, A. O. Ogunfowokan, M. A. Eleruja, and E. E. Ebenso, Int J Electrochem Sc 9 (6), 3008 (2014).
[37] Y. Unutulmazsoy, R. Merkle, D. Fischer, J. Mannhart, and J. Maier, Phys Chem Chem Phys 19 (13), 9045 (2017).
[38] Phil Beauchamp, *Spectroscopy Data Tables: Infrared Tables*. (California State Polytechnic University, 2004).
[39] P. Gupta, A. C. Dillon, A. S. Bracker, and S. M. George, Surf Sci 245 (3), 360 (1991).
[40] K Wende, P Williams, J Dalluge, W Van Gaens, H Aboubakr, J Bischof, T von Woedtke, SM Goyal, KD Weltmann, A Bogaerts, K Masur, and PJ Bruggeman, Biointerphases 10 (2) (2015).
[41] M. Nara and M. Tanokura, Biochem Bioph Res Co 369 (1), 225 (2008).
[42] B. Wichterlova, P. Sazama, J. P. Breen, R. Burch, C. J. Hill, L. Capek, and Z. Sobalik, J Catal 235 (1), 195 (2005).
[43] J. Shibata, K. Shimizu, S. Satokawa, A. Satsuma, and T. Hattori, Phys Chem Chem Phys 5 (10), 2154 (2003).
[44] K. H. Hou and R. Hughes, Chem Eng J 82 (1-3), 311 (2001).
[45] H. Lee, D. H. Lee, Y. H. Song, W. C. Choi, Y. K. Park, and D. H. Kim, Chem Eng J 259, 761 (2015).
[46] C. Yang, Woll, C., Advances in Physics: X 2 (2), 373 (2017).
[47] J. Zarfl, D. Ferri, T. J. Schildhauer, J. Wambach, and A. Wokaun, Appl Catal a-Gen 495, 104 (2015).
[48] K. S. Smirnov and G. Raseev, Surf Sci 384 (1-3), L875 (1997).
[49] J. Kim, D. B. Go, and J. C. Hicks, Phys Chem Chem Phys 19 (20), 13010 (2017).
[50] A. A. Khassin, B. L. Pietruszka, M. Heintze, and V. N. Parmon, React Kinet Catal L 82 (1), 131 (2004).
[51] Y. R. Zhu, Z. H. Li, Y. B. Zhou, J. Lv, and H. T. Wang, React Kinet Catal L 87 (1), 33 (2005).
[52] W. Somers, A. Bogaerts, A. C. T. van Duin, and E. C. Neyts, Applied Catalysis B-Environmental 154, 1 (2014).